Clays and Clay Minerals, Vol. 61, No. 2, 107–132, 2013.

THERMAL HISTORY OF LOWER PALEOZOIC ROCKS ON THE PERI-TORNQUIST MARGIN OF THE EAST EUROPEAN CRATON (PODOLIA, UKRAINE) INFERRED FROM COMBINED XRD, K-Ar, AND AFT DATA

Jan Środoń[1], Mariusz Paszkowski[1], Daniel Drygant[2], Aneta Anczkiewicz[1], and Michał Banaś[1]

[1] Institute of Geological Sciences, Polish Academy of Sciences – Research Centre in Kraków, ul. Senacka 1, 31-002 Kraków, Poland

[2] Natural History Museum of National Academy of Sciences of Ukraine, 18 Teatralna St., 79008 L'viv, Ukraine

Abstract—The Upper Silurian–Lower Devonian section of the Dniester gorge in Podolia and samples from boreholes located S and N of this area were studied in order to reconstruct the thermal history of Lower Paleozoic sedimentary rocks in the Dniester segment of the Peri-Tornquist margin of the East European Craton which is the most eastern part of a major shale-gas target in Europe. X-ray diffraction data for illite-smectite from shales and carbonates indicate very advanced diagenesis and maximum paleotemperatures of ~200ºC, higher than interpreted from the 'conodont alteration index' (CAI) data. Diagenesis of the Devonian section is slightly less advanced than that of the underlying Silurian section, indicating that it is a regional feature and the result of burial. The regional distribution of the diagenetic grade based on illite matches well with the pattern established from the CAI data. K-Ar dating of illite-smectite from Silurian bentonites and shales gave a consistent set of dates ranging from 390 to 312 Ma. To explain such advanced levels of diagenesis and such K-Ar dates, the extension of the Carboniferous foreland basin (which today is only preserved to the NW of L'viv) toward the SE on the craton margin has to be assumed. The diagenetic zonation pattern of the Carboniferous coals supports this hypothesis. The Carboniferous cover may have been either sedimentary or partially tectonic (Variscan intracratonic duplexes) in origin and the thickness, necessary for the observed level of diagenesis, may have been reduced by an elevated heat flow along the major tectonic zone at the edge of the craton (TESZ). The presence of such cover is confirmed by completely reset Cretaceous apatite fission track (AFT) ages of the Silurian bentonites. The AFT dates also imply a Tertiary heating event in the area.

The 10 Å clay mineral present in the dolomitic part of the profile (Silurian), both in bentonites and in other rocks, is aluminoceladonite or intermediate between illite and aluminoceladonite, while in the Devonian shale section only illite was documented. Chlorite is also common in the studied rocks and is at least partially authigenic. It is non-expandable in the samples from boreholes, while often expandable to variable extents in the samples from outcrops, which also contain goethite. Such variation in chlorite is attributed to contemporary weathering.

Key Words—AFT, Aluminoceladonite, Chlorite Weathering, Illite, K-Ar, Peri-Tornquist Margin, Podolia, Shale Gas, Silurian, Thermal History, Ukraine.

INTRODUCTION

The East European Craton (thereafter EEC), also called Baltica, is a fragment of Archean–Mid-Proterozoic crystalline continental crust, ~2500 km across, acting as a separate block of the lithosphere for ~750 Ma, *i.e.* since break-up of the Rodinia mega-continent (*cf.* Nawrocki and Poprawa, 2006), with the sedimentary cover starting in the Riphean and preserved to different degrees mostly in intracratonic and marginal basins (Nikishin *et al*., 1996). The 2000 km long SW margin of the craton (called the Peri-Tornquist margin) faces the Teisseyre-Tornquist Zone (TTZ), also known as the Trans-European Suture Zone (TESZ: *e.g.* Skompski *et al*., 2008; Drygant, 2011), which is the major tectonic line dividing the European crust of Precambrian age from that of younger consolidation (Nawrocki and Poprawa, 2006). The Peri-Tornquist margin encompasses four major sedimentary basins (Figure 1): the Baltic basin in the NW, the Podlasie basin, the Dniester slope, and the Moldova platform in the SE (Vishnyakov *et al*., 1981).

Sedimentation on the Peri-Tornquist margin started in the Riphean and was renewed in the Ediacaran (Vendian) or in the Cambrian (only in the Baltic basin). The Ediacaran continental clastics and flood basalts are interpreted as products of a Neoproterozoic rifting phase, preceding the opening of the Tornquist ocean. Lower Paleozoic sedimentation followed a similar pattern in all basins, interpreted as passive margin types (low sedimentation rate) in Cambrian and Ordovician (sandstones, shales, and carbonates). A rapid increase in sedimentation rate followed in the Silurian (shales and carbonates) due to flexural bending of the craton margin (Nikishin *et al*., 1996; Nawrocki and

* E-mail address of corresponding author:
ndsrodon@cyf-kr.edu.pl
DOI: 10.1346/CCMN.2013.0610209

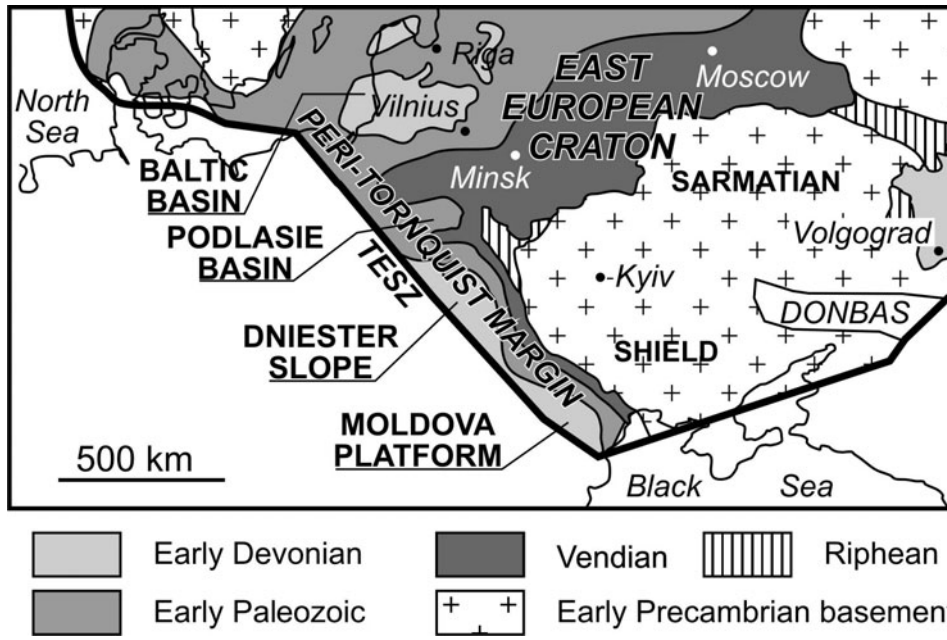

Figure 1. Location of the Dniester slope on the Peri-Tornquist margin of the East European Craton. Map of SW part of the craton (without late Paleozoic and younger cover) adapted from Sliaupa *et al*. (2006). TESZ – Trans European Suture Zone.

Poprawa, 2006; Sliaupa *et al*., 2006). The carbonate-dominated sedimentation continued in the Silurian in the shallowest NE zone of the craton margin (Garetsky *et al*., 1981; figure 8 of Sliaupa *et al*., 2006; Drygant, 2011).

The Lower Paleozoic shales of the Peri-Tornquist margin are currently the major shale-gas target in Europe (Poprawa, 2010), which has led to an increased interest in their diagenetic history. A synthetic study based on the CAI and vitrinite reflectance (R_o; Nehring-Lefeld *et al*., 1997) revealed a systematic zonation in the degree of diagenesis along the entire margin, including its Ukrainian part (CAI data from Drygant, 1993). The interior of the craton has yielded CAI values of 1–1.5 (for Ordovician–Devonian), indicative of paleotemperatures between 50 and 90ºC, according to the CAI calibration of Epstein *et al*. (1977). Toward the SW the CAI values (for the Ordovician) gradually increase and reach 5 (300–480ºC) in the TESZ. This picture is consistent with the parallel increase in R_o from 0.5 to 4.6. In addition, in the Baltic basin sector of the margin, analogous zonation was established from the X-ray diffraction (XRD) evaluation of the composition of illite-smectite (percent smectite layers: %S) in shales (Środoń *et al*., 2009a).

The Silurian and Ordovician rocks of the margin contain numerous bentonite horizons with pure diagenetic illite-smectite, which offer an opportunity for K-Ar dating of the maximum paleotemperatures (Środoń *et al*., 2002), *i.e.* dating the main episode of hydrocarbon generation. In the Baltic basin the K-Ar ages of illite-smectite from bentonites range from 404 to 294 Ma and on the craton margin they are interpreted as indicative of a deep burial under the Devonian and Carboniferous sedimentary cover (Środoń *et al*., 2009a), which is consistent with the geological data (Ulmishek, 1990). Farther to the SE such data are lacking.

A unique opportunity for such a geochronological study on the Dniester slope (Figures 1, 2a) is offered by the ~250 m thick carbonate section of the Upper Silurian (Ludlow and Pridoli), exposed in the banks of Dniester gorge in the Kamyanets Podilsky area (Figure 2b), where numerous bentonite beds can be sampled (Tsegelnjuk, 1980a, 1980b). The beds contain a typical bentonitic mineral assemblage: highly illitic illite-smectite, sometimes of a 1*M* polytype, K-feldspar, quartz, biotite, apatite, and zircon (Huff *et al*., 2000; Kipli *et al*., 2000). In this study these bentonite beds are used for K-Ar dating of illite-smectite, and for AFT dating, while the accompanying shales and overlying Lower Devonian massive shales are used to evaluate the maximum paleotemperatures based on %S (Środoń, 2007).

The combination of XRD, K-Ar, and AFT is a powerful set of methods for basin history studies. The maximum paleotemperatures estimated from XRD and their ages measured by K-Ar have to be consistent with the age and paleotemperature estimations from AFT. The apatite fission tracks anneal completely above 120ºC (Naeser, 1981). Thus, the AFT measurement indicates whether the sample has been buried to temperatures >120ºC (total reset of the original age of the apatite crystal) and when it passed the 120ºC isotherm for the last time on its way to the surface. Such an approach has produced very consistent results

https://doi.org/10.1346/CCMN.2013.0610209 Published online by Cambridge University Press

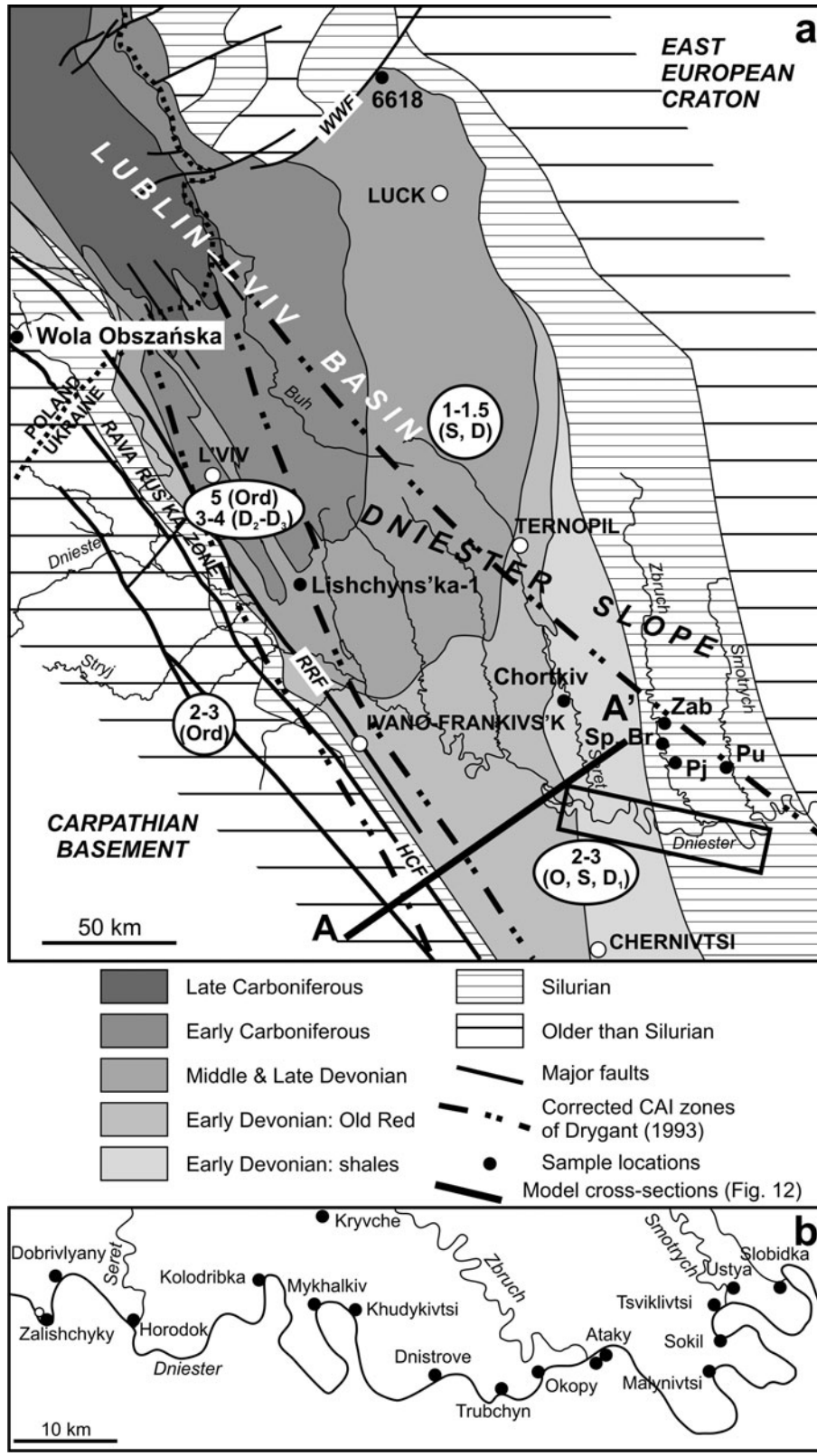

Figure 2. Sample location on the geological map without post-Paleozoic cover (a), compiled from Pożaryski and Dembowski (1983) and Buła and Habryn (2011), and on detailed map of the Dniester gorge and its tributaries (b).

https://doi.org/10.1346/CCMN.2013.0610209 Published online by Cambridge University Press

for the Baltic basin (Środoń *et al.*, 2009a) and for the Miocene Podhale basin (Środoń *et al.*, 2006a; Anczkiewicz *et al.*, 2005). In the present study the same approach was applied to evaluate the maximum burial temperatures of the Lower Paleozoic rocks of the Dniester slope and to date this thermal event.

Table 1. Location, lithology, and stratigraphic position of all the samples studied.

Locality	Sample no.	Lithology	Location	Strat. position
Silurian of Dniester Gorge				
Pudlovtsy quarry	Pu-1	bentonite	2 km N of Kamieniec Podilski	Ludlow
Slobidka outcrop	SM-1	bentonite	48º34′ 31.7″; 26º42′ 14.3″	Ludlow
	SM-3	carbonate below		
	SM-4	carbonate		
Ustya outcrop	Us-1	bentonite		Ludlow
	Us-2	carbonate above		
Tsviklivtsi outcrop	Tsv-1	soft mudstone	48º33′ 45.0″; 26º37′ 44.8″	Ludlow
	Tsv-6	soft mudstone		
	Tsv-7	soft mudstone		
	Tsv-8	soft mudstone		
Sokil outcrop	Sok-1	bentonite	48º32′ 02.5″; 26º37′ 43.4″	Ludlow
	Sok-2	dark bent. above		
	Sok-4	shale	48º32′ 00.8″; 26º37′ 46.7″	
	Sok-5	carbonate		
	Sok-6	carbonate concretion		
Malynivtsi outcrop	Mal-1	bentonite	48º30′ 19.4″ 26º36′ 23.3″	Ludlow
	Mal-2	bentonite		
	Mal-3	bentonite		
	Mal-4	bentonite		
	Mal-5	bentonite		
	Mal-6	bentonite		
	Mal-7	dark bentonite		
	Mal-8	carbonate		
	Mal-10	shale		
Ataky outcrop	At-1	shale		Ludlow
	At-3	carbonate below		
	At-4	bentonite		
	At-9	bentonite		
	At-11	green bentonite		
	At-12	yellow bentonite		
	At-12A	yellow bentonite		
	At-14	soft mudstone	48º32′ 32.2″; 26º27′ 53.3″	
	At-16	bentonite		
	At-18	shale		
Piatnichany outcrop	Pj-1	shale	Zbruch bank	Pridoli
Okopy outcrop	Ok-1	shale below		Pridoli
	Ok-2A	bentonite		
	Ok-2B	bentonite		
	Ok-3	carbonate above		
Trubchyn outcrop	Tr-1	shale	48º31′ 05.9″; 26º19′ 26.8″	Pridoli
	Tr-2	bentonite		
	Tr-4	soft mudstone		
	Tr-5	soft mudstone		
	Tr-6	soft mudstone		
	Tr-7	soft mudstone		
	Tr-8	carbonate		
	Tr-9	bentonite		
Skala Podilska quarry	SP-1	black shale		Pridoli
	SP-3	carbonate		
	SP-4	soft mudstone		
Skala Podilska quarry	SP-8	carbonate		Pridoli
	SP-9	shale		
Bridok quarry	Br-1	soft mudstone		Pridoli
	Br-2	shale		
Zabnitsa outcrop	Zab-1	shale	Zbruch bank	Pridoli

https://doi.org/10.1346/CCMN.2013.0610209 Published online by Cambridge University Press

Table 1 (*contd*)

Locality	Sample no.	Lithology	Location	Strat. position
Devonian of Dniester Gorge				
Dnistrove	Dn-1	shale	48º32′ 16.9″; 26º14′ 21.4″	S/D border
	Dn-3	shale		1.5m above
Mykhalkiv	Myk-1	shale	48º36′ 50.7″; 26º05′ 17.2″	Borshchiv Mb.
Khudykivtsi	Khud-3	shale	48º37′ 09.0″, 26º07′ 29.1″	Khudykivtsi Mb.
Kryvche	Kryv-3	shale	48º42′ 12.4″; 26º05′ 59.1″	Borshchiv Mb.
Kolodribka	Kolod-2	shale	48º33′ 48.9″; 26º03′ 25.8″	Borshchiv Mb.
Chortkiv	Chort-1	shale	48º58′ 15.5″; 25º48′ 53.1″	Chortkiv H.
Horodok	Hor-1	shale	48º37′ 30.3″; 25º52′ 02.4″	Chortkiv H.
Dobrivlyany	Dobr-1	shale	48º40′ 41.5″; 25º36′ 41.0″	Ivanie H.
Zalishchyky	Zalish-1	shale	48º37′ 50.8″; 25º44′ 13.1″	Ivanie H.
	Zalish-3	shale		Dniester ser.
Borehole samples			depth (m)	
6618	6618/9	shale	146.2	Lower Devonian
	6618/5	shale	155.8–158.7	Lower Devonian
	6618/6	shale	167.8–167.9	Lower Devonian
	6618/7	shale	172.55–172.65	Lower Devonian
	6618/10	shale	172.9	Lower Devonian
	6618/11	shale	179.5	Silurian
Lishchyns'ka-1	Lish-1	shale	3300-3306	Silurian

MATERIALS AND METHODS

Samples of the Upper Silurian bentonites, carbonates, soft mudstones, and shales were collected from eight locations in the Dniester gorge and from one location in its tributary Zbrutch gorge (Figure 2b; GPS locations and stratigraphic position given in Table 1). Seven additional samples from six locations nearby were provided by S. Skompski. Fifty seven samples were first investigated as random powders of the bulk rock by XRD in order to identify and quantify their mineral composition and to select samples for clay-fraction separation. The technique of Środoń *et al*. (2001) and the *QUANTA* computer program (Mystkowski *et al*., 2002) were used for the quantification.

Twenty one of the purest bentonite samples and 26 other rocks were selected for clay-fraction separation. The full Jackson (1975) procedure was applied and the <0.2 μm fractions were separated by centrifugation. The <0.2 μm fractions of six bentonite samples underwent further separation into 0.2–0.05, 0.05–0.02, and <0.02 μm fractions by flow-through ultracentrifugation (details in Środoń *et al*., 2006b). Both the <0.2 μm and finer fractions, all in Na form, were subjected to K-Ar dating, following the standard procedure (Środoń *et al*., 2006b). Na-exchanged and not natural samples were used for dating in order to avoid any exchangeable K, which could potentially reduce the measured ages. %S was measured by several peak-positions techniques (Środoń, 1984; Dudek and Środoń, 1996; Środoń *et al*., 2009b) from the XRD patterns of the random bulk-rock air-dry preparations and from the glycolated oriented preparations of the <0.2 μm fractions, recorded with MoS_2 as the internal standard:

(1) Two-peak technique (Dudek and Środoń, 1996, figure 5), which uses peaks of the glycolated <0.2 μm fractions at 15.3–17.9 and 25.9–26.9º2θ (CuKα).

(2) Experimental regressions of %S *vs.* peak position, established from the data of Środoń *et al*. (2009b, table 6). The %S from the Δ2 technique is considered the most accurate and is used as the 'true value' in the regressions. Such regressions are applied to several reflections of the glycolated <0.2 μm fractions and also to the low-angle reflection of the air-dry illite-smectite, measured from the XRD patterns of the bulk rocks, under the assumption that Ca is the dominant natural exchange cation in these rocks with abundant carbonates.

Ten shale samples were collected from the overlying Lower Devonian (Lochkovian) shale and shale-carbonate section, ~530 m thick (Drygant, 2010, figure 1.10), exposed in the Dniester gorge between Dnistrove and Zalishchyky (Figure 2b). They were processed in the same way as the Silurian shales and their <0.2 μm fractions were investigated by XRD, in order to evaluate the degree of diagenesis (%S). Additionally, the same technique was applied to one sample of a Silurian shale from the deeper, shale zone in the TESZ (borehole Lishchyns'ka-1), one Lower Devonian shale from the area north of the Dniester gorge (Chortkiv outcrop), and five Lower Devonian plus one Silurian shale samples from borehole 6618, located in the northernmost part of the Dniester slope (Figure 2a).

Scanning electron microscopy (SEM) was used to study the morphology and composition of adularia identified by XRD in bentonites, to discriminate between Ca-dolomite and ankerite, and to observe the texture of soft mudstones.

https://doi.org/10.1346/CCMN.2013.0610209 Published online by Cambridge University Press

Coarse, clay-free fractions of six bentonites were separated for the adularia study. The other samples were investigated by SEM as bulk rocks.

Apatites were separated for AFT dating from five bentonite samples, using standard crushing, sieving, magnetic, and heavy-liquid (tetrabromoethane and diiodomethane) separation techniques. Polished grain mounts were etched for 20 s in 5 N HNO_3 at 20ºC. The standard glass CN5 was used as a dosimeter to monitor the neutron flux. Thin flakes of low-U muscovite were used as external detectors. Samples together with age standards (Fish Canyon, Durango, and Mount Dromedary apatite) and Corning glass CN5 dosimeters were irradiated with a thermal neutron nominal flux of 9×10^{15}n/cm^2 at the Oregon State University TRIGA reactor (USA). After irradiation, muscovite external detectors were etched for ~45 min in 40% HF in order to reveal the induced tracks. Spontaneous and induced tracks were counted by optical microscopy at 1250× magnification using a NIKON Eclipse E-600, equipped with motorized stage, digitizing tablet, and drawing tube (used for measuring the track length) controlled by the program *FTStage* 3.12 (Dumitru, 1993). Data analyses and age calculations based on a ζ value for CN5 (ζ_{CN5}) of 344±5 were calculated using the program *Trackkey* (Dunkl, 2002).

All quoted AFT ages are 'central ages' (weighted mean ages) in the sense of Gailbraith and Laslett (1993) ±1σ, and the variation of single-grain ages was assessed using the chi-square test (Galbraith, 1981; Green, 1981). The AFT dating followed the procedure described in detail by Anczkiewicz (2005).

RESULTS

Mineral composition of the bulk rocks

The bulk-rock data were grouped by the type of rock (Table 2). For each rock type the samples are arranged by stratigraphic position, starting from the oldest. The Silurian and Devonian shales are presented separately. In the Silurian rocks, the component listed as dolomite is either true dolomite or Ca-dolomite, as identified by XRD and confirmed by energy dispersive X-ray spectroscopy (EDS). A full compositional range of Ca-dolomites is present (104 reflection from 2.884 to 2.903 Å: *cf.* McCarty *et al*., 2006).

Silurian bentonites. 1*M* or 1*Md* illite-smectite dominates the composition: 64−99%. Calcite ranges from 0 to 24%, adularia from 0 to 14%, and quartz from 1 to 7%. Other minerals are traces, except for elevated chlorite and $2M_1$ mica content in At-16. No mineral compositional trend was observed with respect to the stratigraphic position.

Silurian shales. In the Dniester gorge samples, 1*M*d illite is the dominant component: 30−58%, but accompanied by 6−14% of $2M_1$ mica and 4−10% of chlorite. Quartz and K-feldspar increase down the section, 11−19% and 2−22%, respectively. Calcite and dolomite show opposite trends: 0−3% and 34−1%, respectively, down the section. Albite and pyrite are present, but as minor components. Goethite was identified in only one sample. The Silurian shale from the CAI = 5 zone (Lish-1) differs from the Dniester samples in terms of elevated chlorite and albite contents.

Devonian shales. 1*M*d illite is slightly less abundant than in the Silurian section: 22−47%, accompanied by more $2M_1$ mica and chlorite: 5−19% and 4−13%, respectively. Quartz is clearly more abundant: 11−26%, but K-feldspar is low, only reaching the minimum levels of the Silurian section at the base. Calcite and dolomite both increase down the section, but, unlike the Silurian shales, calcite is more abundant: 1−55% and 0−8%, respectively. Albite and pyrite are present as minor components as in the Silurian shales. Goethite is absent, but hematite is present in the uppermost sample, representing the Old Red facies (Dniester series).

Silurian carbonates. Calcite or dolomite are the dominant minerals: 89−63% and 67−45%, respectively. Admixtures of dolomite in limestone and calcite in dolomite are very minor. Other major components are 2:1 clays (1*Md* illite +$2M_1$ mica: 4−28%) and quartz (2−23%). K-feldspar is more abundant than albite, and goethite is absent. The only apparent correlation is that of more chlorite in dolomites than in limestones.

Silurian soft mudstones. The mineral composition of these rocks is intermediate between carbonates and shales. Often both calcite and dolomite are present in significant quantities. Quartz and K-feldspar increase down the section, just as in the shales. Goethite is often observed. As in the carbonates, a positive correlation of chlorite and dolomite content is observed.

Mineral composition of the <0.2 μm fraction of bentonites

The <0.2 μm fractions of all 21 bentonite samples are essentially mono-mineral illite-smectite, without even traces of other clays. The XRD patterns of all Malinovtsy plus Ataki 12 and 12a samples contain a trace of a 3.07 Å peak (Figure 3, jarosite?). Glycolated patterns provide evidence of highly illitic ordered illite-smectite, of ~1−15%S (Figure 3). The greatest degree of illitization was recorded in the center of the thickest bentonite bed (Malinovtsy).

The results for air-dry and glycolated samples are well correlated, but not identical (Table 3). The air-dry values are systematically higher. Differences between values based on the reflections from glycolated patterns are substantial for the most illite-rich compositions. The regression based on the 15.3−17.9º2θ reflection gives negative values for the most illitic samples, which were

https://doi.org/10.1346/CCMN.2013.0610209 Published online by Cambridge University Press

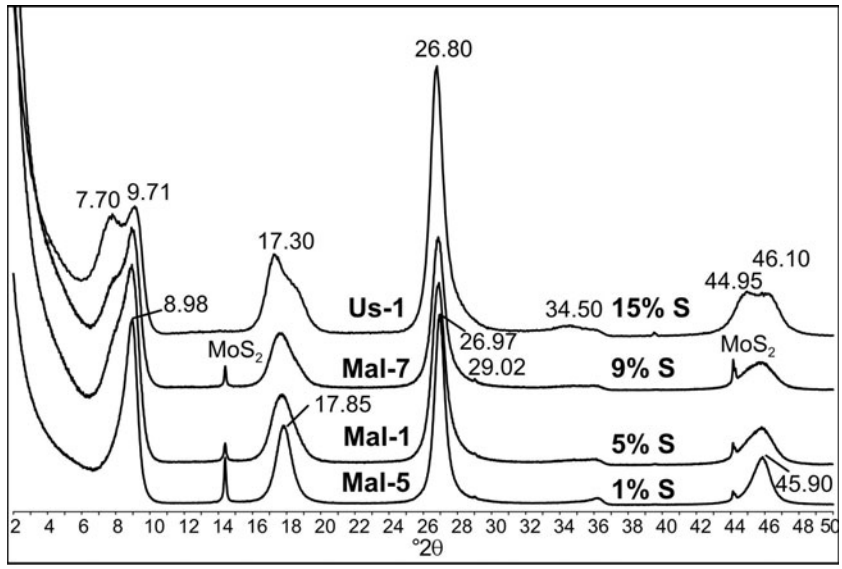

Figure 3. Oriented XRD patterns of glycolated <0.2 μm fractions of the Silurian bentonites, representing the range of expandability of illite-smectite (%S) encountered in this study. Synthetic MoS_2 was added as an internal standard for correcting peak positions.

not accounted for when calculating the mean. These negative values indicate that the measured 2θ values of this reflection are greater than expected for pure K-illite, indicating a smaller thickness of the unit cell of this illite. Indeed, 9.888 Å was measured from 005 for the almost non-expandable illite sample (Mal-6 in Figure 4). Such a small value may imply a significant contribution from fixed Na^+ (the d_{001} value of paragonite is 9.6 Å), but $\%Na_2O$ determinations (Tables 3 and 4) did not reveal elevated Na. The sample was, thus, identified as close to the end-member aluminoceladonite (9.885–9.887 Å: Seifert, 1968; Drits *et al*., 2010). Such identification has been confirmed by Fourier-transform infrared spectra (M. Szczerba, pers. comm.).

In the thick Malinovtsy bed a clear tri-dimensional zonation, perfectly correlated with %S was observed (Figure 4). The polytype evolves from well ordered 1*Mtv* (trans-vacant octahedral sheet) in the lower part of the bed (Mal-6) changing gradually to more disordered structures toward the top of the bed (Mal-1) and abruptly toward the bottom. The tri-dimensional organization of illite-smectite from all thin bentonite beds is of the 1*Md* type, without clear differences in terms of %S. A significant displacement of the 112 peak toward lower

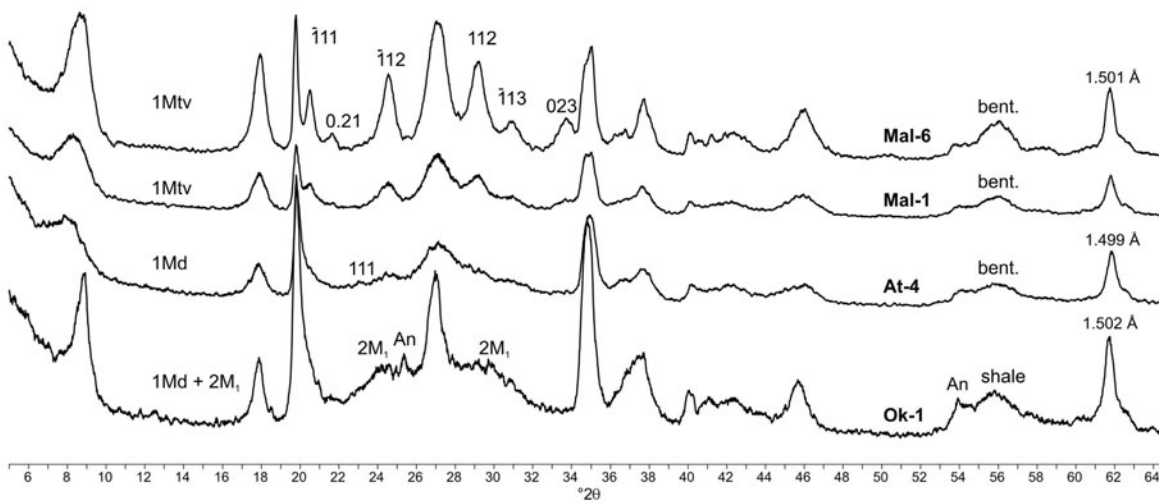

Figure 4. Random XRD patterns of air-dry <0.2 μm fractions of the Silurian bentonites and a shale, representing the detected range of tri-dimensional organization of illite-smectite: from 1*M* to 1*Md* in bentonites, and $1Md + 2M_1$ in shales and other rocks. An – anatase.

https://doi.org/10.1346/CCMN.2013.0610209 Published online by Cambridge University Press

Table 2. Quantitative mineral composition of the rocks studied. Dolomite includes Ca-dolomite if present. H in the goethite row denotes hematite.

Silurian bentonites

	Pu-1	SM-1	Us-1	Sok-1	Sok-2	Mal-1	Mal-2	Mal-3	Mal-4	Mal-5	Mal-6	Mal-7	At-4	At-9	At-11	At-12	At-12A	At-16	Ok.-2A	Ok.-2B	Tr-9	Av. bentonite
Quartz	1.2	1	3.6	2.2	2.8	1.7	1.6	1.8	1.4	1.7	1.1	5.2	5.3	1.9	1.1	2	1.1	4.2	2.9	2.1	6.8	3
Kspar	10.5	4.9	4.9	7.3	8.9	3.9	2	1.6	2.3	3.2	3.7	5.7	6.1	0	0	0.2	0	4.5	14	10.6	4.7	5
Albite	0	0	0	0	0	0	0	0	0	0	0	0	3.6	0	0	0	0	2.4	0	0	0	0
Calcite	0	0	2.1	4.3	8.3	0	0	0	0	2.5	1.1	10.2	0.1	0	0	0.3	0	0	1.5	0.5	24.2	3
Dolomite	0.4	0	0	0	0	0	0	0	0	0	0.4	0	0	0	0	0	0	0	0	0	0	0
Pyrite	0	0.5	0	0	0	0	0.4	0	0.6	0	0	0	0	0	0	0	0	0.3	0	0	0	0
Goethite	1.8	0	0	0	0.7	0.1	0	0	0	0	0	0.1	0.2	0	0	0	0	0	0.7	0.6	0.6	0
Anatase	0	0.7	0	0	0.1	0	0	0	0	0.1	0	0	0	0	0	0	0	0	0.3	0.2	0.2	0
Illite-smectite	86.1	92.8	89.3	86.1	79.1	94.2	96	96.5	95.7	92.5	93.1	78.7	81.6	98	98.9	97.5	98.8	78.9	80.5	85.9	63.5	89
Muscovite	0	0	0	0	0	0	0	0	0	0	0	0	3.2	0	0	0	0	8.6	0	0	0	1
Chlorite	0	0	0	0	0	0	0	0	0	0	0	0	0	0	0	0	0	1.2	0	0	0	0
Biotite						trace																

Silurian shales

	Sok-4	Mal-10	At-1	Zab-1	Ok-1	Tr-1	SP-1	SP-9	Br-2	Lish-1
Quartz	19.2	17.6	8.9	10.5	12.3	11.7	12.1	10.6	11.5	22.8
Kspar	7.6	22.2	9.3	8.8	6.6	2.5	3.7	1.8	3.4	1.1
Albite	4	1.8	3.1	0.2	2.4	2.4	1.5	1.8	3	6.3
Calcite	3.4	2.3	0.1	0.3	0	0	0	0	0.1	3.9
Dolomite	3.1	1.3	36	12.8	5.6	30.3	33.6	34.3	34.2	1.2
Pyrite	0.2	0.5	0.1	0.7	0.1	0.4	0	0.1	0.4	1.6
Goethite	0	0.4	0	0	0	0	0	0	0	0
Anatase	0.2	0.3	0	0	0	0	0	0.4	0	0
Illite	48.4	39.8	30.9	45.4	58	35.3	30.1	35.7	33.1	34.4
Muscovite	6.3	9.6	6	14.3	11	7	10.1	9.4	6.3	14
2:1 clays	54.7	49.4	36.9	59.7	69	42.3	40.2	45.1	39.4	48.4
Chlorite	7.6	4.2	5.3	6.8	4	10.3	8.8	6	8	15
Clay	62.3	53.6	42.2	66.5	73	52.6	49	51.1	47.4	63.4

Devonian shales

	Dn-1	Dn-3	Kryv-3	Khud-3	Myk-1	Kolod-2	Chort-1	Hor-1	Dobr-1	Zalish-1	Zalish-3
Quartz	19.2	16.4	10.7	17.5	11.4	13.2	20.7	26.2	24.9	25.5	25.6
Kspar	3.6	3.8	0.5	0.9	0	0.1	1.5	0	0.1	0.9	0.9
Albite	5.2	3.7	2.2	3.5	1.8	0.5	4.2	4.6	6.4	2.5	5.9
Calcite	26.2	26.2	50.8	20.9	55.1	17	2.1	1	1.3	0.5	2
Dolomite	4	7	0	7.8	0.3	0.2	0.3	0.1	0.2	0	0
Pyrite	0.1	0.1	0.1	0.3	0.3	0.1	0.2	0	0.5	0.4	0
Goethite	0	0	0	0	0	0	0	0	0	0	3.6 (H)
Anatase	0	0.2	0	0	0	0.4	0	0	0.4	0.3	0

Illite-smectite	30.4	26.2	24.2	28.2	22.3	42.1	47.4	39.5	36.1	41	36.3
Muscovite	5.9	11	7.4	10.8	5.2	13.7	11.8	16.8	18.1	19.4	16.2
2:1 clays	36.3	37.2	31.6	39	27.5	55.8	59.2	56.3	54.2	60.4	52.5
Chlorite	5.4	5.4	4	10.2	3.6	12.8	11.7	11.9	12	9.6	9.4
Clay	41.7	42.6	35.6	49.2	31.1	68.6	70.9	68.2	66.2	70	61.9

Silurian carbonates

	SM-3	Us-2	Sok-5	Sok-6	Mal-8	At-3	Ok-3	Tr-8	SP-3	SP-8	av. Lime	av. Dolo
Quartz	15.8	7.7	6.7	2.3	22.9	4.2	10.1	4.2	12.2	12.3	9	11
Kspar	5.3	1.1	1.8	0.3	1.9	6.7	4.2	0.8	1.6	3.6	1	4
Albite	2.9	1	0	0.4	0.6	0.9	1.6	0.6	1.9	2	1	2
Calcite	0.1	73.7	63	83.1	63.9	0.4	0.2	88.9	8.9	1.3	75	2
Dolomite	48.5	1.8	1.8	0	0.3	76.3	44.8	0.4	57.9	48.3	1	55
Pyrite	0.2	0.1	0.4	0	0	0.1	0	0.5	0.4	0.3	0	0
Goethite											0	0
Anatase	0	0	0	0	0	0.6	0	0.2	0	0	0	0
Illite	14.6	11.7	17.5	9.4	7.6	6	15.6	4.2	9.7	20.3	10	13
Muscovite	7.2	0.7	5.3	1.3	2.8	0.3	12.5	0	0.6	5.9	2	5
2:1 clays	21.8	12.4	22.8	10.7	10.4	6.3	28.1	4.2	10.3	26.2	12	19
Chlorite	5.5	2.2	3.4	3.2	0	4.4	11	0	6.7	6.1	2	7
Clay	27.3	14.6	26.2	13.9	10.4	10.7	39.1	4.2	17	32.3	14	25

Silurian soft mudstones

	SM-4	Tsv-6	Tsv7	Tsv-8	At-14	Pj-1	Tr-2	Tr-4	Tr-5	Tr-6	Tr-7	SP-4	SP-7	Br-1	av. Lime.	av. Dolo.
Quartz	13.6	24.8	18.7	23.5	14.8	9.2	8	8.6	13.4	7.4	7.8	11.6	13.2	10.6	9	16
Kspar	5.8	7.5	6.1	3.6	4.1	3.6	3.8	1.4	2.8	2.4	1.5	2.8	2.7	3.7	2	5
Albite	3	2.5	3	1.9	2.7	2.5	1.3	0.9	3.7	1.1	2.1	2	1.5	1.9	1	3
Calcite	0	8.1	11.7	14.5	0.2	1.4	64.2	52.7	16.6	61.5	67.2	29.4	45	0	53	7
Dolomite	18.3	18.9	27.2	32	45.9	54.3	4.2	16.3	45.2	10.4	0.1	0	0.2	59.6	5	38
Pyrite	0.3	0	0.1	0.3	0.1	0	0.1	0.1	0	0	0	0.1	0	0	0	0
Goethite			1.4	1.7			0	0	0	0.6	0.5	0.2	0		0	0
Anatase	0	0.2	0	0.1	0	0	0.2	0	0	0.2	0	0	0.3	0.2	0	0
Illite	36.5	25.3	19	7.6	21.8	20.4	13.4	14.1	14.4	9.7	13.9	31.4	29.9	10.6	19	19
Muscovite	14	7.6	8.3	8.1	6.7	4.7	4.6	5.7	0.7	3.8	6.7	17.3	7.1	5.7	8	7
2:1 clays	50.5	32.9	27.3	15.7	28.5	25.1	18	19.8	15.1	13.5	20.6	48.7	37	16.3	26	26
Chlorite	8.6	5.1	4.3	6.8	3.6	3.8	0.3	0.3	3.3	3.1	0.1	5	0.3	7.7	2	5
Clay	59.1	38	31.6	22.5	32.1	28.9	18.3	20.1	18.4	16.6	20.7	53.7	37.3	24	28	32

Table 3. XRD data for illite-smectite: 00l reflections from air-dried bulk rock and glycolated <0.2 μm fractions of Silurian bentonites: peak positions (º2θ) and percent smectite (%S) calculated from these peak positions using experimental regressions derived from data of Środoń *et al.* (2009) or obtained ($\%S_{DS}$) from figure 5 of Dudek and Środoń (1996). $\%Na_2O$ refers to the <0.2 μm fraction.

Location	Sample no.	1 AIR	$\%S_{AIR}$	1 GLY	%S	3 GLY	%S	5 GLY	$\%S_{DS}$	6 GLY	%S	7 GLY	8 GLY	8 GLY-7 GLY	%S	Mean $\%S_{GLY}$	$\%Na_2O$
		2θ		2θ		2θ		2θ		2θ		2θ	2θ	2θ			
Pudlovtsy	Pu-1	8.08	**17**	8.1	9	17.58	7	26.82	6	34.92	10					**8**	
Slobidka	SM-1	8.18	**14**	7.9	12	17.5	10	26.8	8	34.85	11					**10**	
Ustye	Us-1	8	**19**	7.7	16	17.3	16	26.8	13	34.5	18	44.95	46.1	1.15	14	**15**	0.15
Sokil	Sok-1	8.14	**16**	7.8	14	17.3	16	26.8	13	34.5	18	44.95	46.1	1.15	14	**15**	0.13
	Sok-2	8.18	**14**	7.8	14	17.3	16	26.8	13	34.5	18	44.95	46.1	1.15	14	**15**	
Malynivtsi	Mal-1	8.3	**11**	diffuse		17.73	1	26.89	2	34.77	13					**5**	
	Mal-2	8.3	**11**	diffuse		17.73	1	26.95	2	34.77	13					**5**	0.11
	Mal-3	8.52	**5**			17.85	-4	26.95	1	35.18	5					**3**	0.09
	Mal-4	8.62	**2**			17.85	-4	26.97	1							**1**	0.13
	Mal-5	8.74	**0**			17.85	-4	26.97	1							**1**	
	Mal-6	8.66	**1**			17.85	-4	26.97	1							**1**	0.07
	Mal-7	8.3	**11**	7.93	12	17.61	6	26.89	5	34.77	13					**9**	
Ataky	At-4	8.06	**18**	7.8	14	17.42	12	26.78	10	34.68	15					**13**	
	At-9	8.2	**14**	7.96	11	17.58	7	26.84	6	34.9	10					**9**	0.13
	At-11	8.16	**15**	7.9	12	17.42	12	26.78	10	34.68	15					**12**	0.09
	At-12	8.14	**16**	7.9	12	17.42	12	26.78	10	34.68	15					**12**	
	At-12A	8.22	**13**	7.9	12	17.42	12	26.78	10	34.68	15					**12**	0.12
	At-16	8.26	**12**	7.9	12	17.58	7	26.84	6	34.9	10					**9**	
Okopy	Ok-2A	8.26	**12**	8.02	10	17.48	10	26.82	9	34.84	11					**10**	
	Ok-2B	8.26	**12**	8.02	10	17.48	10	26.82	9	34.84	11					**10**	
Trubchyn	Tr-9	8.36	**9**	8.08	9	17.76	0	26.82	2							**4**	0.13

Bold indicates the most important values, *i.e.* those discussed in the text.

Table 4. XRD data for air-dry and glycolated <0.2 μm fractions of shales and carbonates (marked with *): angular positions of 001 reflections of illite (1AIR and 1GLY) and their difference, d_{001} illite calculated from 005 reflection, Intensity ratio, Ir (Środoń, 1984), Kubler (KI) index for air-dry sample, peak broadening of 002 chlorite reflection, semiquantitative estimate of chlorite abundance (swelling chlorites marked with **). For 3 samples also measurable positions of IS reflections and percent smectite calculated from 6GLY (comp. Table 2).%Na_2O refers to the <0.2 μm fraction.

Location	Sample no.	1AIR °2θ	1GLY °2θ	Δgly-air °2θ	3GLY °2θ	6GLY °2θ	%S	d_{001} (Å)	Ir	KI °2θ	FWHM002ch °2θ	Chlorite content	%Na_2O
Silurian of Dniester Gorge													
Słobidka	SM-3*	8.82	8.86	0.04				9.931	1.14	0.71	0.65	xx**	0.13
	SM-4*	8.82	8.88	0.06				9.935	1.02	0.65	0.49	xx**	
Ustye	Us-2*	8.84	8.88	0.04				9.964	1.28	0.38	0.25	xxx	
Sokil	Sok-4	8.82	8.90	0.08				9.927	1.17	0.64	0.80	x**	
	Sok-5*	8.82	8.86	0.04				9.935	1.23	0.71	0.64	xx**	
	Sok-6*	8.76	8.88	0.12				9.91 & 9.96	1.23	0.71	0.35	xxx**	
Malynivtsi	Mal-8*	8.7	8.88	0.18				9.931	1.64	0.98	0.73	x**	
	Mal-10	8.76	8.84	0.08				9.935	1.30	0.82	0.67	x**	
Ataky	At-1	8.76	8.84	0.08				9.939	1.31	0.78	0.55	x	
	At-3*	8.8	8.84	0.04				9.935	1.23	0.78	0.44	x	
	At-18	8.8	8.86	0.06				9.939	1.17	0.73	0.53	x	
Okopy	Ok-1	8.76	8.86	0.10				9.939	1.24	0.87	0.50	tr	0.13
	Ok-3*	8.82	8.90	0.08				9.931	1.38	0.73		xx**	0.12
Trubchyn	Tr-1	8.82	8.86	0.04				9.939	1.06	0.55	0.51	x**	
	Tr-8*	8.78	8.86	0.08				9.943	1.38	0.75		xx**	
Skala Podilska	SP-1	8.84	8.86	0.02				9.943	1.11	0.55	0.51	x	
	SP-3*	8.8	8.86	0.06				9.951	1.22	0.82	0.58	xx	0.15
Devonian of Dniester Gorge													
Dnistrove	Dn-1	8.72	8.88	0.16				9.943	1.32	0.82	0.53	xx	
	Dn-3	8.82	8.88	0.06				9.955	1.20	0.73	0.36	xx	
Mykhalkiv	Myk-1	?	8.88					9.960	1.12	0.71	0.22	xxx	
Khudykivtsi	Khud-3	8.80	8.92	0.12				9.947	1.56	0.82	0.44	xx	
Kryvche	Kryv-3	8.76	8.92	0.16				9.947	1.62	0.95	0.53	xx	
Kolodribka	Kolod-2	8.62	8.86	0.24				9.947	1.64	1.04	0.56	xx	
Chortkiv	Chort -1	8.70	8.88	0.18				9.955	1.68	1.15	0.67	xx	
Horodok	Hor-1	8.76	8.88	0.12				9.955	1.49	0.96	0.60	xx	
Dobrivlyany	Dobr-1	8.70	8.88	0.18				9.955	1.40	0.96	0.58	xx	
Zalishchyky	Zalish-1	8.70	8.86	0.16				9.955	1.43	0.96	0.53	xx	
	Zalish-3	8.70	8.86	0.16				9.955	1.44	0.96	0.58	xx	
Borehole samples													
6618	6618/9	8.76	8.86	0.10		34.72	14	9.960	1.72	1.00	kaol	kaol	
	6618/5	8.48	8.88	0.40	17.10	33.94	29	9.960	2.56	1.49	kaol	kaol	
	6618/6	8.66	8.90	0.24	17.08	34.18	24	9.951	1.69	1.35	0.42	x	
	6618/7	8.72	8.86	0.14				9.955	1.36	1.15	0.32	x	
	6618/10	8.86	8.90	0.04				9.951	1.46	1.00	0.21	xx	
	6618/11	8.80	8.88	0.08				9.960	1.62	0.98	0.30	xx	
Lishchyns'ka-1	Lish-1	8.80	8.80	0.00				9.951	1.01	0.29	0.15	xxx	

angles with respect to the *tv* peak position, a greater relative intensity of $\bar{1}13$, and the appearance of a 111 peak (At-4 in Figure 4) indicate ~50% of the *cv* component (*cis*-vacant octahedral sheet: Moore and Reynolds, 1997, figure 10.18). The 34–38º2θ region indicates clear domination of $n{\cdot}120^{\circ}$ rotations (Moore and Reynolds, 1997, figure 10.14). The d_{006} value (2θ value normalized to a ZnO internal standard) evolves systematically from 1.499 Å for most random samples to 1.501 Å for the most ordered structures.

Mineral composition of the <0.2 μm fraction of other rocks

Silurian of the Dniester gorge. Twenty-two samples of the Silurian shales, carbonates, and soft mudstones collected close to the bentonite beds were investigated for their clay mineral composition. All <0.2 μm fractions contain dominant illite and variable amounts of chlorite. In a few carbonate and soft mudstone samples a smectitic component was also detected.

The XRD characteristics of illite in all samples except two (Us-2 and Sok-6) are very similar. Only a trace amount (<<5%) of swelling layers can be detected by comparing air-dry and glycolated patterns normalized to the MoS_2 internal standard (Table 4, Tr-8 in Figure 5). The position of the 001 peak of the air-dry illite moves by Δgly-air = 0.02–0.18º2θ toward higher angles after glycolation and its intensity decreases slightly. The 002 and 005 peaks change very slightly and the 003 increases in intensity and moves slightly toward lower angles. The Ir index based on these changes (Środoń, 1984) varies from 1.64 to 1.06, which are values characteristic of almost non-expandable illites. The Kübler index (KI; Kübler, 1964), measured for <0.2 μm air-dry Na-samples, ranges from 0.98 to 0.55º2θ. The d_{001} value of these illites can be evaluated from the 005 reflection as 9.91–9.95 Å, *i.e.* much lower than the standard K-illite value of 9.98 Å (Lindgreen *et al.*, 2000), but higher than the measured bentonite value of 9.888 Å, thus indicating an intermediate illite-aluminoceladonite composition (Drits *et al.*, 2010).

Sample Us-2 contains illite, which is perfectly non-expandable (no shift in peak positions after glycolation), has thicker crystals (KI = 0.38), and d_{001} = 9.964 Å (Table 4, Figure 5). Sample Sok-6 is clearly heterogeneous, with both illitic (9.96 Å) and aluminoceladonitic (9.91 Å) components (Table 4, Figure 5).

The d_{006} values of illites in non-bentonitic samples are ~1.502 Å (Figure 4). Random XRD patterns of all samples in the 20–38º2θ range are very similar to sample Ok-1 (Figure 4) and are indicative of the mixture of dominant 1*Md* with minor $2M_1$ polytype, with more $n{\cdot}60^{\circ}$ rotations than the bentonitic samples (single peak at 35 and increased intensity at 37.2º2θ: Moore and Reynolds, 1997; figure 10.14). The sample Us-2 contains more $2M_1$ in the <0.2 μm fraction than other samples and does not contain an increased number of $n{\cdot}60^{\circ}$ rotations.

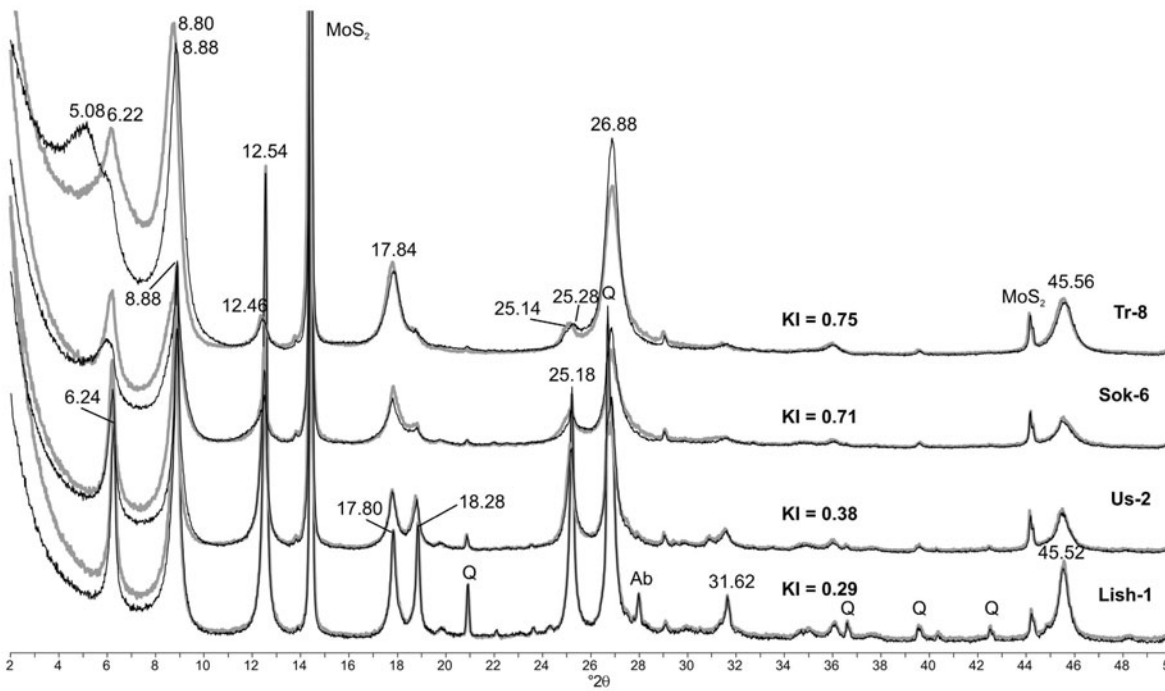

Figure 5. Oriented XRD patterns of air-dry (gray) and glycolated (black) <0.2 μm fractions of the Silurian non-bentonitic rocks, representing the range of illite and chlorite crystal size and swelling encountered. KI – Kübler index.

https://doi.org/10.1346/CCMN.2013.0610209 Published online by Cambridge University Press

Chlorites are found in quite variable amounts (Table 4, Figure 5). In some samples chlorites are perfectly non-expandable: their d_{001} value is close to 14.1−14.3 Å and does not shift after glycolation. The intensity of the 001 and 002 reflections are very close, indicating Mg-chlorite (Moore and Reynolds, 1997). Chlorite from sample Us-2 is exceptional: more Fe-rich (002 stronger than 001) and coarser (narrower reflections: Figure 5). Broadening of the 002 chlorite reflection, measured in the air-dry state (FWHM002ch in Table 4), is substantially smaller than that of 001 illite (KI).

Most samples contain chlorite, which is slightly expandable. Expandability is shown by a variable shift of 001 (to 15.1 Å in the extreme case: Table 4), by a similar shift of 002, and by the shift of 004 in the opposite direction (Sok-6 in Figure 5), which are consistent (Mering rule) with interlayering of a minor ~17 Å (smectitic) swelling component.

The d_{006} values of most chlorites vary in the 1.535−1.530 Å range (Mg-chlorites), except for sample Us-2 (1.542 Å), which is consistent with more Fe (Wiewióra and Wilamowski, 1996).

In four samples a phase with a dominant smectitic swelling component occurs along with a separate chloritic phase, both contributing to the 14 Å reflection in the air-dry state (Tr-8 in Figure 5). The presence of both minerals becomes clearly visible after glycolation. The smectitic phase is identified by its broad ~17.4 Å peak (Tr-2 and 8, Ok-3) or a diffuse band >14 Å (SP-4) and raised intensity after glycolation in the 9.5−11, 15−17, and 25.5−26.5º2θ range. The heterogeneous nature of these minerals is supported by their poorly defined peaks. For sample Tr-2 with the best-defined peaks, the 15−17º2θ band starts clearly from 5.67 Å, which is less than the 003 peak from 17.4 Å, indicating that even in this sample some degree of mixed layering is present. Mixed layering of the expandable layers with chlorite layers was also shown by a 300ºC heating test. The low-angle peaks disappeared, but the intensity increased (a raised 'saddle') between the chlorite and illite 001 reflections.

Sample Tr-2 looks to be entirely dioctahedral, based on the d_{006} region. In the other samples, weak tri-octahedral reflections between 1.534 and 1.525 Å are visible.

Lower Devonian shales of the Dniester gorge. The XRD characteristics of Lower Devonian shales are very similar to the Silurian shales with non-expandable chlorite. Illite is also almost non-expandable (<<5%S), but all characteristics indicate slightly more expandability than in the Silurian shales: Δgly-air from 0.06 to 0.24, Ir from 1.12 to 1.68, and KI from 0.71 to 1.15 (Table 4). The d_{001} value of these minerals ranges from 9.94 to 9.95 Å, indicating a pure illitic composition. The chlorites are non-expandable and Mg-rich. Sample Myk-1 is exceptional, with more chlorite, which is more coarse-grained and Fe-rich.

Borehole samples. The XRD characteristics of samples from borehole 6618 indicate greater illite expandability than the Lower Devonian shales of the Dniester gorge: Δgly-air from 0.04 to 0.40, Ir from 1.36 to 2.56, and KI from 0.98 to 1.49 (Table 4). For the three uppermost samples, the diagnostic IS reflections were measurable, allowing the estimation of %S from 14 to 29 (Table 4). In two uppermost samples, kaolinite was identified. In the remaining samples non-expandable chlorite is present.

The single sample from borehole Lishchyns'ka-1 contains end-member non-expandable illite (Δgly-air = 0, Ir = 1.01, d_{001} = 9.95 Å) with KI = 0.29 (Table 4) and very abundant, extremely coarse-grained Fe-chlorite (Figure 5).

K-Ar dating of illite

Twelve Silurian bentonite samples were dated: six as 0.2−0.05, 0.05−0.02, and <0.02 μm sub-fractions, and six as <0.2 fractions (Table 5). The dates from the subfractions range from 340 to 390 Ma and the dates of the <0.2 μm fractions also fall within this range. The oldest date was recorded for the finest fraction (Mal-5), thus the whole range can be considered as representing pure diagenetic ages (Środoń *et al*., 2002). No systematic geographic variation of ages can be observed.

K-Ar dating was also performed for clay fractions of six Silurian samples representing other lithologies: limestones, a calcite concretion, and soft mudstones. The <0.2 and 2−0.2 μm fractions were used for dating (Table 5). All the dates are close to the bentonite ages with most close to the highest value but three even lower than the youngest bentonite age (312, 325, and 334 Ma). The samples with the most coarse-grained illite (sharpest XRD peaks: Us-2 and Sok-6) gave the oldest dates (378 and 397 Ma), but even those are much younger than the stratigraphic age (417−423 Ma).

AFT dating

Five Silurian bentonite samples were examined by AFT. The AFT data are listed (Table 6) and presented as radial plots (Galbraith, 1990) (Figure 6). All analyzed samples yielded Upper Cretaceous pooled ages (63−107 Ma), significantly younger than the estimated stratigraphic age (417−423 Ma). The dispersion of ages between individual apatite crystals is large, as indicated by small P(χ^2) values (Table 6). The measured ranges (Figure 6) are quite similar (~210−40 Ma) for all samples except for SM-1 (350−50 Ma). These measured ages are younger than the stratigraphic age and younger than the K-Ar ages of the maximum temperatures.

All of the samples examined provided small numbers of confined tracks (Table 6, Figure 7). The mean length of confined tracks per sample ranges from 9.50 to 13.48 μm. The track-length distributions are either symmetric (Mal-1 and Zab-1) or skewed toward small track length (Sok-1 and SM-1). The Pu-1 distribution is

https://doi.org/10.1346/CCMN.2013.0610209 Published online by Cambridge University Press

Table 5. K-Ar dates of fine fractions of bentonites and other Silurian rocks.

Sample no.	Fraction (μm)	Weight (mg)	% K_2O	% $^{40}Ar^*$	$^{40}Ar^*$ (pmol/g)	Age (Ma)	Error (Ma)
Silurian bentonites							
Pu-1	0.2–0.05	39.75	7.35	89.41	4087.7	350	2
Pu-1	0.05–0.02	71.35	7.18	86.08	3881.8	341	2
Pu-1	<0.02	38.60	7.13	88.31	4012.6	354	2
SM-1	<0.2	24.38	6.73				
SM-1	0.2–0.05	62.50	6.87	92.26	4125.6	375	2
SM-1	0.05–0.02	29.75	6.71	93.05	4113.5	382	2
SM-1	<0.02	22.15	6.62	83.55	3581.9	341	2
Us-1	<0.2	20.1	6.53	85.16	3560.5	344	2
Sok-1	<0.2	19.15	6.44	79.17	3558.4	348	2
Sok-1	<0.2	20.9	6.44	78.53	3555.3	348	2
Mal-5	<0.2	30.01	7.56				
Mal-5	0.2–0.05	57.40	7.83	91.90	4273.5	344	2
Mal-5	0.05–0.02	14.85	7.52	87.04	4547.9	378	2
Mal-5	<0.02	47.40	7.31	90.97	4581.0	390	2
Mal-7	0.2–0.05	37.25	7.17	89.50	4098.5	359	2
Mal-7	0.05–0.02	19.60	6.29	80.88	3383.2	340	2
Mal-7	<0.02	31.45	6.94	90.91	3738.4	340	2
At-12	0.2–0.05	32.60	7.20	89.76	3936.3	345	2
At-12	0.05–0.02	21.8	6.88	90.11	3902.6	356	2
At-12	<0.02	34.1	6.89	87.62	3711.8	340	2
At-4	<0.2	24.95	6.42	86.03	3506.6	344	2
Ok-2A	0.2–0.05	36.25	6.91	89.69	3704.6	339	2
Ok-2A	0.05–0.02	22.70	6.89	91.19	4017.3	339	2
Ok-2A	<0.02	32.20	6.85	92.18	3721.2	339	2
Tr-9	<0.2	29.75	7.08	91.48	3795.6	339	2
Other Silurian rocks							
Us-2	2–0.2	42.65	5.5	89.93	3327.5	378	2
Sok-6	<0.2	24.4	5.6	78.44	3415.8	381	2
Sok-6	2–0.2	36.35	6.17	90.68	3942.9	397	2
Mal-8	<0.2	9.04	5.87	80.39	3013.6	325	4
Mal-8	2–0.2	27	3.37	67.95	1651.6	312	3
Mal-10	<0.2	31.45	6.90	90.09	3388.9	313	2
Tr-2	<0.2	15.65	6.14	78.38	3243.5	334	3
SP-4	<0.2	13.35	6.13	80.92	3697.8	377	3
Standard							
GLO	bulk	100.70	7.90	26.60	1104.8	95	1
GLO	bulk	127.35	7.90	79.15	1132.1	97	1
GLO	bulk	60.05	7.90	87.59	1128.3	97	1

not reliable because too small a number of tracks was available for the measurement.

SEM observations and EDS analyses

In all six bentonite samples (Mal−2, 4, 6, Ok-2B, Sok-1, Us-1), the separated coarse fraction is dominated by adularia, with minor amounts of pyroclastic quartz, biotite, apatite, and zircon. The adularia crystals are isometric and range from 50 to 100 μm in diameter. Growth features are common (Figure 8), but in the Malynivtsi samples are less abundant, which gives these crystals a more regular appearance.

Numerous EDS analyses performed for samples SP-3 and Tr-5 revealed that the carbonate mineral identified by XRD is Ca-dolomite and not ankerite. The texture of soft mudstone was observed in three samples (At-14, SP-4, and Tr-5). The samples are very porous due to partial dissolution of carbonate rhombohedra (Figure 8).

INTERPRETATION

Weathering overprint

Most of the samples studied come from natural outcrops, thus some weathering features can be

https://doi.org/10.1346/CCMN.2013.0610209 Published online by Cambridge University Press

Table 6. AFT results for Podolia Silurian bentonite samples. No. crystals is the number of apatite crystals analyzed for tracks. ρ and *N* are densities of tracks ($\times 10^6$ tracks/cm^{-2}) and numbers of tracks counted, respectively, measured for dosimeter, apatite (spontaneous), and external detector (muscovite: induced). P (χ^2) [%] – homogeneity of the apatite population expressed by χ^2 test (Galbraith, 1981; Green, 1981). Central age and U content calculated using the program *Trackkey* 4.2 (Dunkl, 2002). Number of measured confined tracks in a sample, and their average length are reported also.

Sample no.	No. crystals	Dosimeter		Spontaneous		Induced		P (χ^2) (%)	Age (Ma) ±1σ	Age distribution (Ma)	U (ppm)	No. conf. tracks	Length (μm)
		ρ*d*	*Nd*	ρs	*Ns*	ρ*i*	*Ni*						
Pu-1	13	1.15	5738	1.5618	198	2.9975	380	1.23	102.1±13.8	210–40	31.85	15	9.50±0.87
SM-1	26	1.141	5738	0.1843	120	0.3501	228	31.78	107.5±15.5	350–50	3.77	40	11.87±0.40
Sok-1	16	1.11	5738	0.6118	161	1.1096	292	40.43	105.0±13.5	210–65	12.45	22	12.52±0.28
Mal-1 to 2	20	1.098	5611	0.8401	380	1.5784	714	0.54	99.7±11.4	220–50	17.39	29	13.48±0.30
Zab-1	11	1.155	5738	0.221	45	0.7023	143	49.95	63.1±11.2	200–30	7.41	47	12.08±0.30

expected. The dissolution of carbonate rhombohedra detected by SEM, the presence of goethite and jarosite, the swelling of some chlorites, and the mixed-layer smectite-chlorite (Figure 5) are interpreted as products of contemporary weathering. The association of smectite-chlorite with chlorite, and the presence of swelling chlorite in numerous samples indicate that the smectite-chlorite is a chlorite weathering product. Based on the d_{006} value, these minerals seem to have evolved toward a dioctahedral composition.

Such interpretation is supported by peak broadening of the 002 chlorite reflection (Figure 9) plotted *vs.* KI, which is widely regarded as a key indicator of the degree of deep diagenesis and anchimetamorphism. For a given KI, the chlorites from boreholes have the narrowest peaks. Next are the Devonian chlorites from outcrops and the broadest are the Silurian chlorites from outcrops. This sequence probably reflects the length of exposure to weathering: none in the boreholes, and much shorter on the Devonian shale slopes of Dniester than on the Silurian carbonate vertical walls, which are expected to be much more resistant to erosion (Figure 10). The distribution of goethite (Table 2: common in the Silurian most porous rocks, of mineral composition intermediate between carbonates and shales, and as such the most prone to weathering) supports this interpretation. Thus, chlorite from outcrops should be excluded as an indicator of the diagenetic grade, being non-resistant to weathering.

The swelling minerals detected by Huff *et al*. (2000, figure 6) in the outcrops of the same Silurian section are also probably chlorite weathering products. On the other hand, the core samples from the same stratigraphic interval, farther NW on the Peri-Tornquist margin (Baltic basin), and representing similar diagenetic grade, contain only non-expandable chlorite (Środoń and Clauer, 2001), like the borehole chlorites from this study.

Provenance

The K-Ar dates of clay fractions from the Silurian rocks other than bentonites are predominantly within the values measured for bentonites (Table 5). This is not a common situation: most often the detrital component of epiclastic rocks results in dates significantly older than the dates obtained from the clay fractions of pyroclastics (*e.g.* Clauer *et al*., 1997). Such young ages imply a combination of two factors: the detrital material on the Silurian carbonate platform was predominantly pyroclastic, while the epiclastic component was minor and young (Caledonian). Very similar results were obtained for the Baltic basin segment of the Peri-Tornquist margin (Środoń and Clauer, 2001), both indicating the alimentation of these basins from outside the East European Craton.

Diagenetic phenomena

The high Mg content of the Silurian section is manifested by abundant dolomite/Ca-dolomite in carbo-

https://doi.org/10.1346/CCMN.2013.0610209 Published online by Cambridge University Press

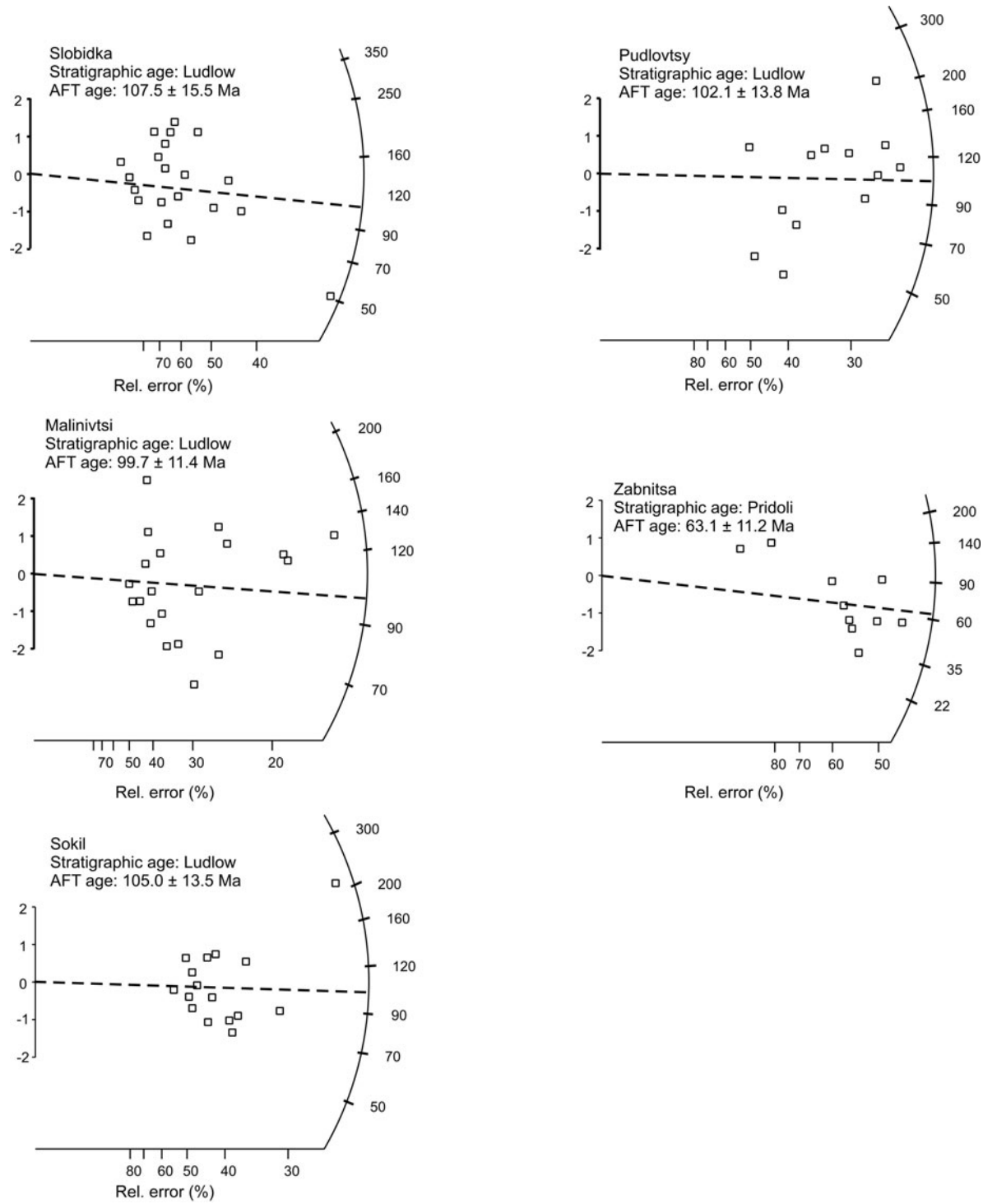

Figure 6. The distributions of AFT ages of individual apatite crystals and central ages of samples (weighted means) presented on the radial plots of Galbraith (1990). The age of each crystal may be determined by extrapolating a line from 0 on the vertical scale of standard deviation (σ) for the sample through the crystal position on the plot (small rectangle) to the radial age scale. Central ages of samples are defined by the dashed lines. The horizontal scale presents the relative error of age estimation for individual crystals, related to the number of measured tracks.

https://doi.org/10.1346/CCMN.2013.0610209 Published online by Cambridge University Press

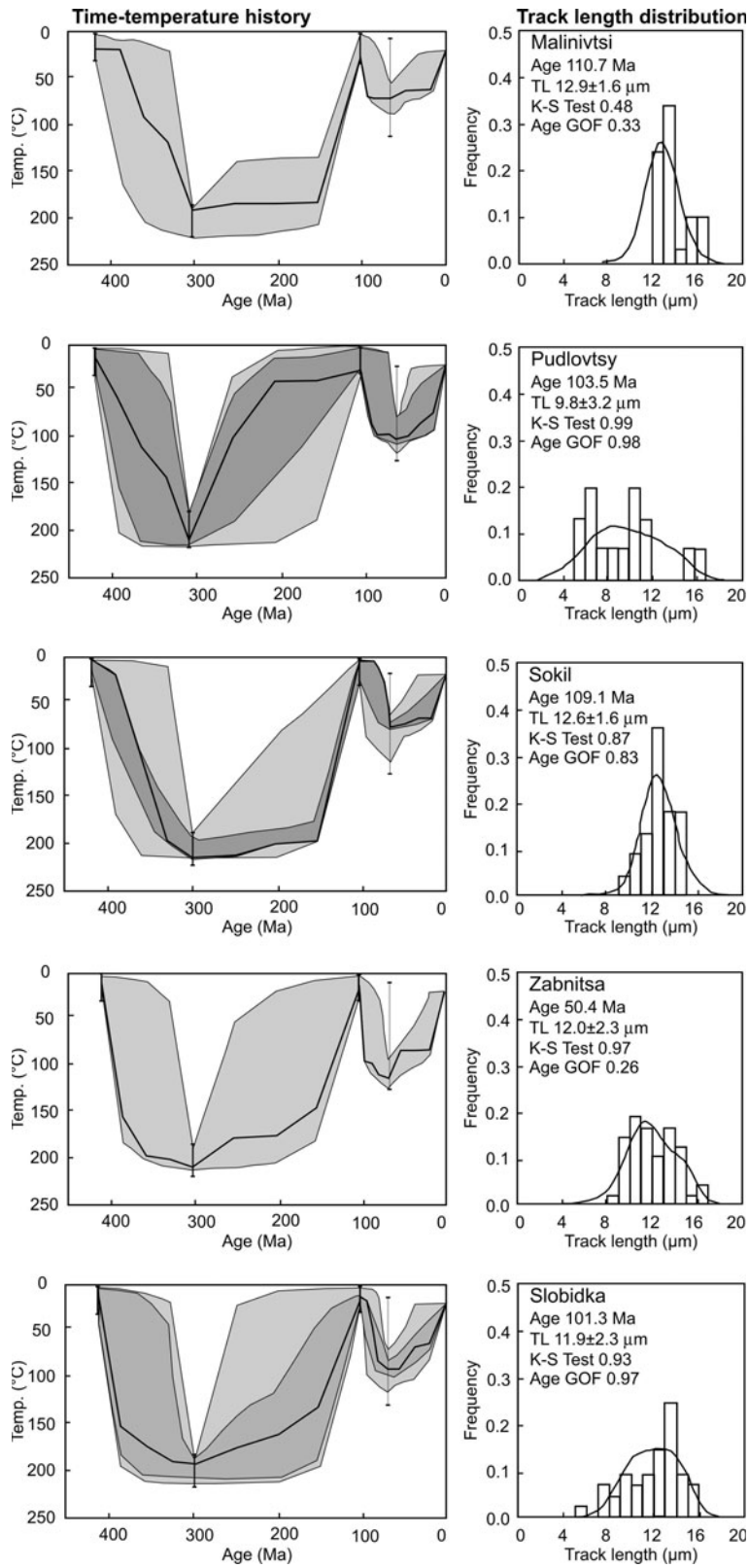

Figure 7. Track-length distributions and models of thermal history obtained using *AFTSolve* (Ketcham *et al*., 2000). In order to explain the observed AFT length distributions, a post-Albian thermal episode has to be assumed.

https://doi.org/10.1346/CCMN.2013.0610209 Published online by Cambridge University Press

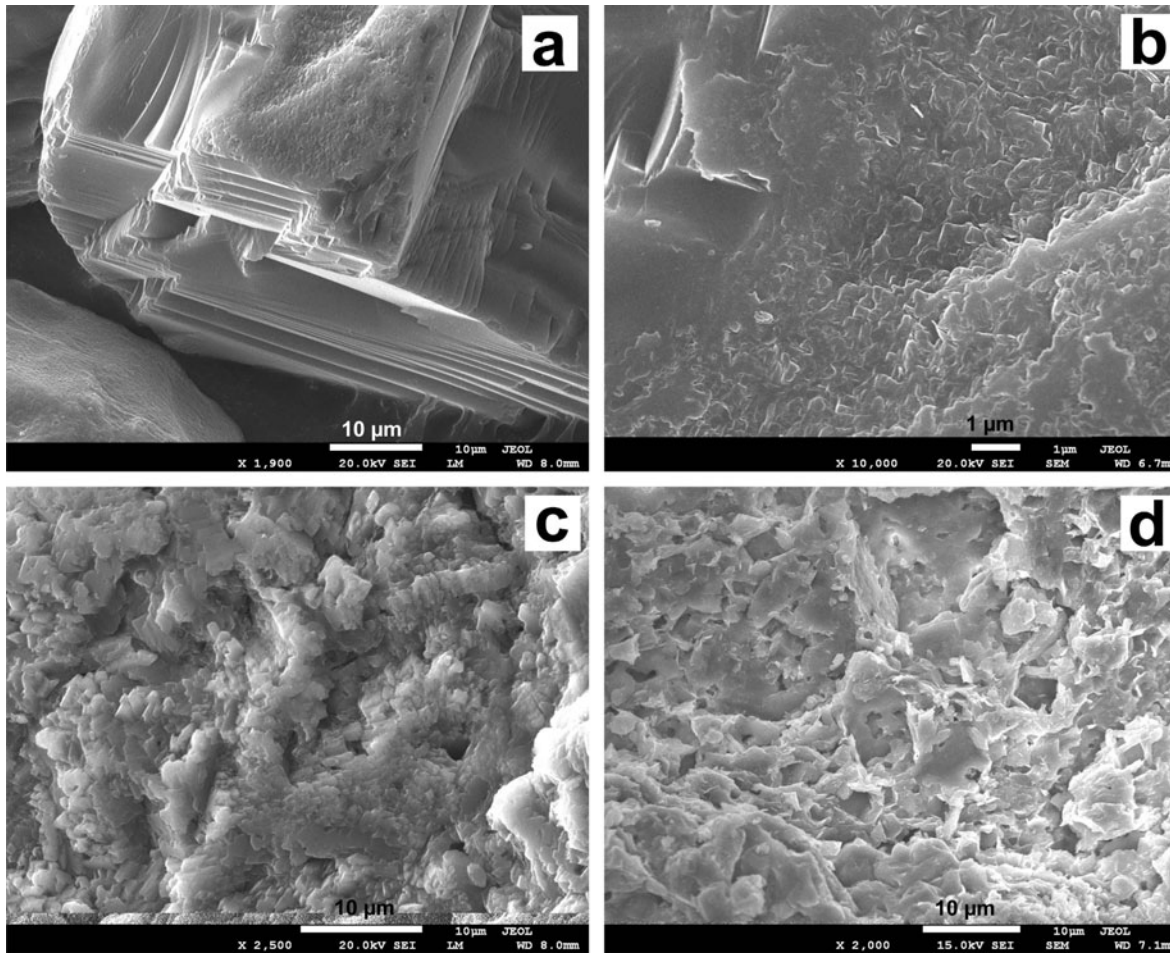

Figure 8. SEM images of growth features at the surfaces of feldspars from bentonites (a–c) and of porosity in soft mudstones, created by the dissolution of carbonate crystals (d).

nates, soft mudstones, and shales; by the Mg-rich composition of the 10 Å mineral (intermediate illite-aluminoceladonite composition) in these rocks; and by a positive correlation of dolomite and Mg-chlorite in carbonates, shales, and soft mudstones (Table 2). In bentonites, both dolomite and chlorite are absent but the

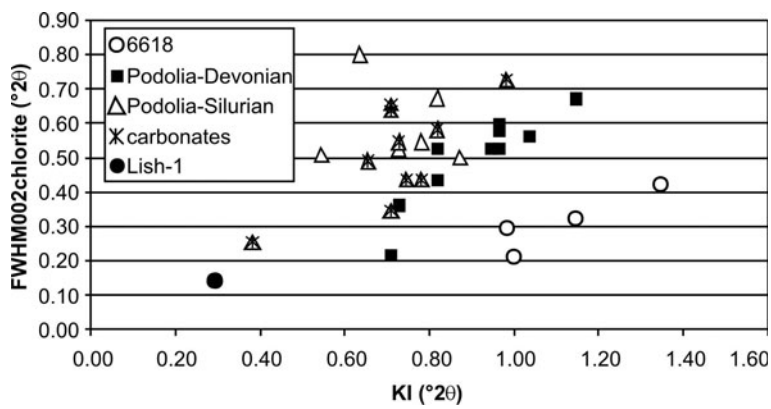

Figure 9. Peak broadening of chlorite 002 reflection (FWHM002chlorite) in non-bentonitic samples (with Silurian carbonates indicated separately), plotted *vs* the Kübler index (KI), regarded as an indicator of the diagenetic grade. For the given KI, FWHM002chlorite is greatest for the most weathered samples.

https://doi.org/10.1346/CCMN.2013.0610209 Published online by Cambridge University Press

Figure 10. Photos illustrating more stable Silurian carbonate slopes (a: near Ustya) and the Devonian shale slopes (b: near Kolodribka) of the Dniester gorge.

illite-smectite is Mg rich and evolves toward pure aluminoceladonite. In the Devonian shales, calcite is abundant, dolomite scarce, and the 10 Å mineral has strictly illitic composition. The bulk-rock composition control over the diagenetic products is, thus, clearly evident.

Diagenetic zonation observed in a thick bentonite bed (Malynivtsi) is the opposite of earlier reports of a lower degree of illitization in the center of bentonite beds (Środoń, 1976; Altaner *et al*., 1984). It resembles the zonation in a sandstone bed (Whitney and Northop, 1987), interpreted as a result of fluid flow through the bed; an explanation difficult to accept for an impermeable bentonite bed, unless it became a shear zone as the least competent layer in this carbonate section, and this zone became a conduit for migrating hot fluids.

Maximum burial temperatures

The %S in illite-smectite of the studied Silurian section preserves the pattern typical of sedimentary basins with the %S in bentonite beds greater than in shales (*cf. e.g.* Šucha *et al*., 1993). Only the most illitized samples of the thick bentonite bed (Malynivtsi) reach the level of illitization typical of shales and other non-bentonitic rocks from this section. Based on the shale values of %S <<5 the maximum paleotemperatures can be evaluated as 200ºC or even slightly higher (Środoń, 2007). K-Ar dates and aluminoceladonitic composition, restricted to the dolomite-dominated (*cf.* Table 2) Silurian sequence, clearly prove that the shale illitic material is predominantly diagenetic and not detrital, and thus suitable for the paleotemperature estimation.

To verify whether the illite-smectite paleotemperature curve, calibrated for regular illite from shale sequences (Środoń, 2007), can also be applied to aluminoceladonite from carbonate sequences, the overlying Lower Devonian shale sequence was studied. The data form trends consistent with the stratigraphic position (more advanced diagenesis of the Silurian rocks: Figure 11a,b), which are bracketed by the Lish-1 anchimetamorphic sample (>250ºC, based on KI = 0.29) and the 24%S sample from borehole 6618, corresponding to 125ºC (Środoń, 2007). Deep burial of both Silurian and Lower Devonian sections of the Dniester gorge to the maximum temperatures of ~200ºC has been confirmed by these data.

The alternative data for the maximum paleotemperature estimation, available from the study area (*cf.* Sachsenhofer and Koltun, 2012), are the CAI measurements of Drygant (1993, and ten additional unpublished measurements from this study area, which modify

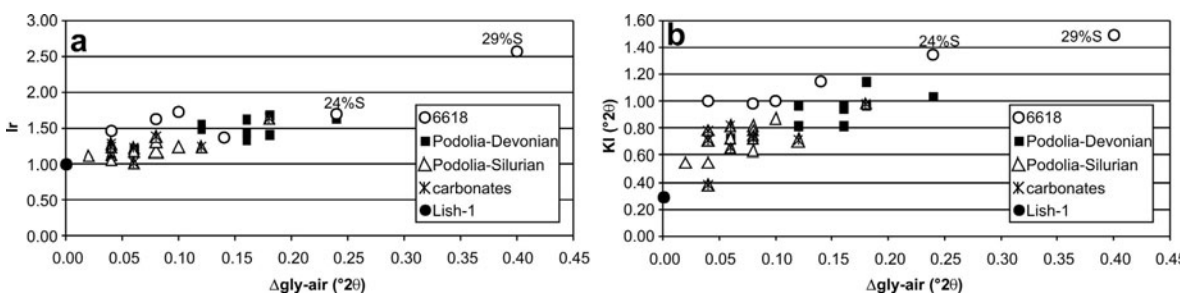

Figure 11. Diagenetic trends in the non-bentonitic samples studied, illustrated by plots of Ir index (Środoń, 1984) and Kübler index (KI) *vs.* difference in XRD 001 peak positions between glycolated and air-dried samples (Δgly-air).

https://doi.org/10.1346/CCMN.2013.0610209 Published online by Cambridge University Press

slightly the original map: Figure 2a). The Dniester section studied gave CAI = 2−3, which, according to Drygant (1993), indicates paleotemperatures up to 200ºC. Nehring-Lefeld *et al*. (1997), who compiled CAI data for the entire Peri-Tornquist margin, interpreted the CAI = 2−3 zone as corresponding to the maximum paleotemperatures of 110−140ºC. According to the authors of the CAI method (Epstein *et al*., 1977), the color of conodonts depends heavily on the heating time, thus the length of the heating period has to be assumed. The K-Ar data indicate 10s of Ma, putting the maximum CAI = 3 paleotemperature well below 150ºC. An analogous discrepancy between %S and CAI estimates of the maximum paleotemperatures has been observed for the Baltic basin (compare figure 4 of Środoń *et al*., 2009a and figure 7 of Bergstrom, 1980).

In Pomerania (Baltic basin), where both CAI and vitrinite reflectance (R_o) data are available (Nehring-Lefeld *et al*., 1997), the CAI = 2−3 zone corresponds to R_o = 1−2, which indicates 140−200ºC maximum paleotemperatures according to Suggate (1998) and 150−250ºC according to Barker and Pawlewicz (1986). In the hot Miocene East Slovak Basin, used for the %S-based paleothermometry (Środoń, 2007), ~5%S and R_o= 2 have been measured in shales currently at 200ºC, at a depth of 4 km (Franců *et al*., 1990).

The AFT ages, which are completely reset (Table 6), suggest that the maximum post-depositional paleotemperatures were >100±20ºC (Naeser, 1981), which is consistent with both the clay and organic-based estimates.

Clay data tend to indicate that the maximum paleotemperatures were slightly higher than the CAI-based values, but the general regional pattern of paleotemperatures recorded by CAI (Figure 2a) is confirmed by the clay data. The Lish-1 anchimetamorphic illite comes from CAI zone 4−5, the samples in the Dniester gorge section with <<5%S in IS correspond to CAI = 2−3, and the samples from the top of 6618 borehole, with 24−29%S in IS, correspond to CAI = 1.5.

A Vendian Al-glauconite from Kytayhorod in the Dniester gorge (15 km E and <200 m below the Silurian in the section) was dated at 360−404 Ma (Gorokhov *et al*., 1997). Those authors interpreted these dates, following Morton and Long (1984), as indicative of resetting due to oxidation during uplift and contact with meteoric waters. These dates are coincident with the illite-smectite diagenetic ages reported here, which probably indicate total or almost total reset of the stratigraphic ages during the deep burial event, suggesting burial conditions close to 250ºC (reset temperature for illite: Hunzicker *et al*., 1986) for the Cambrian-Vendian part of the profile in the Dniester gorge.

Burial and thermal history

Bentonite K-Ar data constrain the age of maximum paleotemperatures at 390−340 Ma (Middle Devonian-Lower Carboniferous). The K-Ar data of clay fractions from shale and limestone from the vicinity of a thick bentonite bed (Malynivtsi) extend the lower limit to 310 Ma (Upper Carboniferous). Together they represent the range of ages very close to those measured for bentonites from Pomerania, *i.e.* another segment of the Peri-Tornquist margin (294−382 Ma: Środoń *et al*., 2009a).

In Pomerania these K-Ar ages are interpreted as representing the maximum burial followed by a long-lasting uplift, based on the regional geology and confirmed by basin modeling (Poprawa *et al*., 2010). The data collected for the Lower Devonian shales from the Dniester gorge verify a deep burial of the section, leading to an analogous conclusion of a long-lasting uplift of the Podolia area, which is corroborated by the available geological data. During the Permian and Mesozoic the entire study area, along with the rest of the Dniester slope, were parts of a much larger landmass, undergoing uplift and erosion. During the late Albian/early Cenomanian (~100 Ma ago) a few tens of meters of shallow marine sediments were deposited in Podolia, and are preserved in the area, though partially eroded (Świdrowska *et al*., 2008). These data imply that the Silurian rocks under study were uplifted from a depth corresponding to 200ºC (5−10 km assuming a feasible range of geothermal gradients from 40 to 20ºC/km) to the surface between 300 and 100 Ma ago. These estimates give the mean rates of uplift of the Dniester gorge area in this period from 25 to 50 m/Ma.

Deep burial conditions during the Carboniferous and Permian are consistent with the paleomagnetic measurements from the Silurian of Podolia, performed on fine-grained diagenetic magnetite, which indicate pervasive remagnetization of this age (Jeleńska *et al*., 2005). On the other hand, the existing geological evidence does not provide an explicit identification of the missing 5−10 km column of the eroded overburden. According to the paleogeographic maps compiled by Nikishin *et al*. (1996) the study area experienced only some coastal zone sedimentation (alluvial-deltaic and shallow-marine sands and shales) during the Early Devonian but became land (no deposition) starting from the Middle Devonian. This reconstruction would be consistent with the K-Ar evidence only if 5−10 km of the Early Devonian cover were originally deposited in this area. The preserved sedimentary record makes such an assumption unlikely. It consists of 530 m of Lochkovian marine shales, siltstones, and limestones (Tyver Superhorizon) and 0−1194 m of Old Red Pragian-Emsian fluvial-estuarine siliciclastics (Dniester Series) with an erosional upper surface (Małkowski *et al*., 2009; Drygant, 2010).

Tectonic burial under Caledonian nappes thrust onto the craton margin from the SW similar to the sequence of events recorded in the Polish sector of the Peri-Tornquist slope (Znosko, 1970) can be excluded, based on the cross-sections of the craton margin constructed for the area (Drygant, 2010). A feasible scenario has to

https://doi.org/10.1346/CCMN.2013.0610209 Published online by Cambridge University Press

assume that the Nikishin *et al*. (1996) reconstruction is not correct and that the entire area of the Dniester slope became a part of the Variscan foreland basin and was covered by a thick Upper Devonian–Upper Carboniferous (+Permian?) cover, the bottom part of which is preserved today as an erosional remnant in the Lublin–L'viv coal basin and farther NW on the Peri-Tornquist slope (Figure 2a). The zonation of Carboniferous coal grade corresponds perfectly to the diagenetic zonation of the underlying Lower Paleozoic strata, as it increases to the SW (Karnkowski 2003; Shulga *et al*., 2007). Also, the thickness of subsequent Carboniferous formations increases to the SW toward the Rava Rus'ka Fault (Shulga *et al*., 2007, figure 34). The SE border of the Lublin-L'viv Basin is erosional, with younger strata intersecting the present-day surface successively toward the NW (Figure 2a). Coals of the Lublin-L'viv Basin are characterized by R_o = 0.55–1.0 (Majorowicz *et al*., 1984), indicative of substantial burial (1.5–3.0 km according to figure 5 of Suggate, 1998). The missing overburden probably included Permian, as indicated by the Permian K-Ar ages of illite-smectite from the Carboniferous sandstones of the Lublin basin (Kozłowska, 2011). 120ºC or occasionally even higher diagenetic temperatures in the Carboniferous rocks were estimated from fluid inclusions in sandstone cements (Kozłowska, 2002; Poprawa and Żywiecki, 2005). Detrital micas, as well as monazite and zircon from the Carboniferous sandstones of the Lublin-L'viv coal basin, give distinctive Carboniferous age cluster, documenting the Variscan source area (Paszkowski and Kusiak, 2005). All these features are consistent with the hypothesis of an asymmetric Upper Paleozoic basin fill, thickest in the SW, extending originally on the Dniester slope toward the SE, at least as far as the Dniester gorge area. This was responsible for the diagenesis of the underlying Lower Paleozoic rocks, and was removed by erosion during the Mesozoic uplift of the area.

Part of this Carboniferous basin, now destroyed by erosion, was probably located in the present-day Rava Rus'ka tectonic zone, bordering the Lublin-L'viv basin from the SW (Figure 2a). Such an hypothesis is supported by the Silurian bentonite K-Ar dating from the Wola Obszańska borehole (Kowalska, 2008), located in this zone just W of the Polish-Ukrainian border (Figure 2a). Four bentonite samples from this profile gave 12–14%S, thus a similar level of burial as the Dniester gorge area, and also a similar illite-smectite K-Ar age range of 285–364 Ma. The %S determinations in Silurian shales from several boreholes in this zone (Kowalska, 2008) indicate a level of diagenesis similar to well 6618, located on the NE edge of the Lublin-L'viv basin (Figure 2a). These data allow speculation that the depocenter of the Carboniferous basin ran NW–SE more or less along the Rava Rus'ka fault, as recorded by the highest CAI values of 5 (Figure 2a). Originally, the axis of this basin may have deepened toward the SE, allowing for thicker Upper Paleozoic overburden than known from the NW (Warsaw-Lublin area), and the tectonic inversion of this basin was stronger in the SE, resulting in deeper exhumation. Such a sequence of events is typical of basins controlled by major faults (*e.g.* Podhale basin: Środoń *et al*., 2006a).

Such narrow depocenters, localized over major faults (Figure 12a) filled with siliciclastics with very high sedimentation rates and high thermal maturity, are known from several parts of Larussia in front of the Variscan orogen (Clare basin in Ireland: Croker, 1995; Culm basin in Cornwall: Warr and Hecht, 1993; Reugen basin in NE Germany: Kornpihl, 2005; Donbas basin in the Ukraine: Reznikov, 1978).

An alternative feasible mechanism, which could have produced excessive burial along the Rava Rus'ka fault is a Variscan intracratonic duplex thrusting event. Such structures have been recognized farther to the NW in Poland along the Ursynów-Kazimierz fault, which is a NW continuation of the Rava Rus'ka fault (Antonowicz *et al*., 2003; Krzywiec, 2009). Similar transpressional thrust duplexes form a newly described class of orogens known as intracontinental transpressional thrust/fault belts (Cunningham, 2005; Cunningham and Mann, 2007). The duplex overburden may have been removed entirely by erosion, due to deeper exhumation of this area (Figure 12b).

Theoretically, such differences in the level of diagenesis could also be attributed to the variation in paleo-heat flow between the platform and TESZ. The thickness distribution of the Carboniferous formations in the Lublin-L'viv Basin, correlating positively with the coal grade, testifies against the heat flow variation as the major factor. Analyses of contemporary heat-flow patterns in Poland did not detect major differences between TESZ and the craton (Majorowicz *et al*., 2003). However, the analysis of vitrinite reflectance profiles from the Lublin basin reveals a systematic increase of the paleogeothermal gradient along the Peri-Tornquist slope (Majorowicz *et al*., 1984, figure 7) from the region near Warsaw (27ºC/km, similar to a contemporary gradient) to the Polish–Ukrainian border (50º/km, twice the contemporary gradient: estimates based on Suggate, 1998, in agreement with the estimates of Majorowicz *et al*., 1984). Botor *et al*. (2002) detected a similar trend in the area. If this trend in the paleogeothermal gradient continued farther to the SE, as implied by the modeling (Karnkowski, 2003), then the estimates of the Carboniferous burial of the L'viv slope presented above could be reduced significantly.

An elevated and variable heat flow along TESZ in the Carboniferous was also proposed by Poprawa and Żywiecki (2005), who explained it by advection in the transpressional stress field. This hypothesis is consistent with the Tournisian bimodal magmatic activity in the Lublin basin (5000 km^2 of basalt and trachyte cover, up

https://doi.org/10.1346/CCMN.2013.0610209 Published online by Cambridge University Press

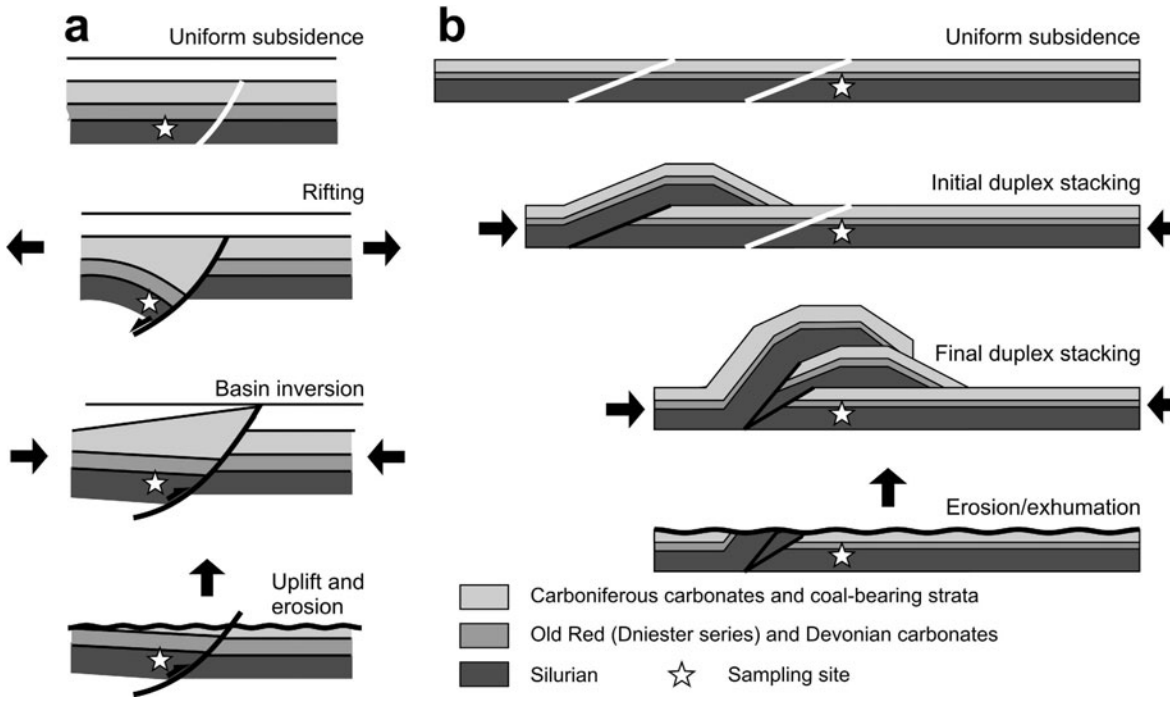

Figure 12. Models (cross-sections along A–A′ trend in Figure 2a) of burial/thermal history of the study area, explaining possible mechanisms of elevated degree of diagenesis along the Rava Rus'ka Fault. Fault-controlled local depocenter formed in transtensional(?) regime, with subsequent inversion and erosional removal of entire anomalously-thick basin fill (a), and intracratonic transpressive(?) duplexing over undeformed basement and subsequent exhumation and erosional removal of entire duplex.

to 230 m thick: Grocholski and Ryka, 1995), and farther to the NW (Jaworowski, 2002; Muszyński *et al*., 1996).

The data presented do not allow for selection of the most feasible scenario or their combination, but they confirm the diagenetic CAI-based zonation (Drygant, 1993) and date the advanced diagenesis on the Dniester slope as Devonian–Carboniferous, thus related to the Variscan orogeny, and induced by the Upper Devonian–Carboniferous overburden and, possibly, tectono-thermal events.

The AFT dates confirm a complete post-depositional reset and slow exhumation (distributions skewed to small track length and shortened tracks: Gallagher *et al*., 1998). Such AFT ages do not represent the age of the crossing 100±20ºC isotherm but are significantly younger (*e.g.* Gallagher *et al*., 1998, figure 4b; Green *et al*., 1989, figure 1). However, the AFT ages measured are much too young to be reconciled with any feasible scenario of the exhumation to surface in the Albian (Świdrowska *et al*., 2008), and then residing in near-surface temperatures, as would be expected from the very thin Cenozoic cover (up to 200 m of Miocene marine sediments: Nowak, 1938). This conclusion was confirmed by the modeling with *AFTSolve* (Ketcham *et al*., 2000), a computer program for deriving thermal history information from the apatite fission-track data. *AFTSolve* generates possible time–temperature paths (Figure 7), using the Monte Carlo algorithm, by fitting the experimental fission-track length distributions with distributions calculated according to the Laslett *et al*. (1987) annealing model. The dark gray areas in Figure 7 mark fields with goodness-of-fit [GOF] $\geqslant$ 0.5, and thick lines correspond to the thermal history with maximum GOF. The light gray fields show imperfect but acceptable models of thermal histories. The original constraints used in modeling were as follows: (1) the stratigraphic ages of samples (~400 Ma); (2) the age of maximum paleotemperatures (from K-Ar dating: ~300 Ma); (3) the age of unroofing to the surface (~100 Ma – the stratigraphic age of overlying Cretaceous sediments); and (4) present-day mean surface temperature.

In order to explain the measured ages and track-length distributions, a post-Albian heating event to ~100ºC must be assumed (Figure 7). Feasible models can be constructed both assuming relatively old and young post-Albian heating events. No independent evidence, supporting such thermal events in the Dniester area, was found in the literature, however.

The burial history inferred here for the Dniester slope bears some close similarities to the history of the Carboniferous fill of Donbas, located 500 km to the east within the Sarmatian Shield (Figure 1). Also, in Donbas, the post-Carboniferous erosion is estimated to have reached 10 km, numerous Cretaceous AFT cooling-ages were measured (Danisik *et al*., 2010) and the

https://doi.org/10.1346/CCMN.2013.0610209 Published online by Cambridge University Press

maximum level of alteration reached the anchimetamorphic stage in the axial zone of the basin (Środoń and Paszkowski, 2011).

CONCLUSIONS

(1) The Silurian and Lower Devonian rocks in Podolia underwent deep burial diagenesis, with maximum temperatures reaching 200ºC.

(2) This diagenetic event lasted from the Upper Devonian to the end of the Carboniferous, based on K-Ar dating of illite-smectite from bentonites and shales. This result implies that the spatial distribution of shale gas *vs*. shale oil rocks in the area is controlled by the Dniester slope evolution during the Upper Paleozoic, which constrains the basin history models for the area.

(3) The spatial pattern of diagenesis detected using illite-smectite corresponds to the CAI data, and implies that the highest diagenetic temperatures occurred along the Rava Rus'ka Fault.

(4) To explain this pattern, the extension of the Carboniferous Lublin-L'viv basin to the SE has to be imagined, possibly with a narrow, fault-controlled depocenter or a transpressional Variscan intracratonic duplex thrust over the Rava Rus'ka Fault zone, which produced anchimetamorphic temperatures. Elevated heat flow may have also played a role.

(5) The long-lasting uplift of the Sarmatian Shield destroyed this thick sedimentary cover in Podolia, as proven by the Cretaceous AFT ages. An additional, much weaker, post-Albian heating period has to be assumed to explain the AFT data fully.

(6) At such a deep level of diagenesis, the bulk-rock composition (carbonate *vs.* shale) does not measurably affect the degree of smectite illitization, but a lower degree in bentonites is still measurable. The bulk-rock chemistry (elevated Mg) resulted in elevated contents of chlorite and affected illite chemical composition, producing aluminoceladonite in the Silurian dolomitic section.

(7) The comparison of core and outcrop samples indicates that chlorite is partially opened during contemporary outcrop weathering and for this reason it is unsuitable as an indicator of diagenetic degree.

ACKNOWLEDGMENTS

Małgorzata Zielińska and Tadeusz Kawiak are thanked for sample preparation and XRD measurements, respectively. Leszek Chudzikiewicz helped with the figures. Stanisław Skompski supplied a set of his Silurian samples. Chevron Laboratories in Houston are acknowledged for permission to use their proprietary *QUANTA* program. Anonymous reviewers offered valuable comments and language corrections, which helped to improve the presentation.

REFERENCES

Altaner, S.P., Hower, J., Whitney, G., and Aronson, J.L. (1984) Model for K-bentonite formation: evidence from zoned K-bentonites in the disturbed belt, Montana. *Geology*, **12**, 412–415.

Anczkiewicz, A.A. (2005) Apatite fission track verification of the maximum paleotemperatures estimated from smectite illitization for the Tatra Mts., Podhale Basin, and the adjacent area of the External Carpathians. PhD thesis, Institute of Geological Sciences PAN, Kraków, Poland, 126 pp. (in Polish).

Anczkiewicz, A.A., Zattin, M., and Środoń, J. (2005) Cenozoic uplift of the Tatras and Podhale basin from the perspective of the apatite fission track analyses. *Mineralogical Society of Poland – Special Papers*, **25**, 261–264.

Antonowicz, L., Hooper, R., and Iwanowska, E. (2003) Lublin Syncline as a result of thin-skinned Variscan deformation (SE Poland). *Przegląd Geologiczny*, **51**, 344–350 (in Polish with English summary).

Barker, Ch.E. and Pawlewicz, M.J. (1986) The correlation of vitrinite reflectance with maximum temperature in humic organic matter. Pp. 79–93 in: *Paleogeothermics* (G. Buntebarth G. and L. Stegena, editors). Lecture Notes in Earth Sciences, Vol. **5**, Springer-Verlag, Berlin.

Bergström, S.M. (1980) Conodonts as paleotemperature tools in Ordovician rocks of the Caledonides and adjacent areas in Scandinavia and the British Isles. *Geologiska Föreningens i Stockholm Förhandlingar*, **102**, 377–392.

Botor, D., Kotarba, M., and Kosakowski, P. (2002) Petroleum generation in the Carboniferous strata of the Lublin Trough (Poland): an integrated geochemical and numerical modelling approach. *Organic Geochemistry*, **33**, 461–476.

Buła, Z. and Habryn, R. (2011) Precambrian and Paleozoic basement of the Carpathian Foredeep and the adjacent Outer Carpathians (SE Poland and Western Ukraine). *Annales Societatis Geologorum Poloniae*, **81**, 221–239.

Clauer, N., Środoń, J., Franců, J., and Šucha, V. (1997) K-Ar dating of illite fundamental particles separated from illite-smectite. *Clay Minerals*, **32**, 181–196.

Croker, P.F. (1995) The Clare basin: a geological and geophysical outline. Pp. 327–339 in: *The Petroleum Geology of Ireland's Offshore* (P.F. Croker and P.M. Shannon, editors). Special Publication **93**, Geological Society, London.

Cunningham, D. (2005) Active intracontinental transpressional mountain building in the Mongolian Altai: Defining a new class of orogen. *Earth and Planetary Science Letters*, **240**, 436–444.

Cunningham, D. and Mann, P. (2007) Tectonics of strike-slip restraining and releasing bends. Pp. 1–12 in: *Tectonics of Strike-Slip Restraining and Releasing Bends* (W.D. Cunningham and P. Mann, editors). Special Publication **290**, Geological Society, London.

Danisik, M., Sachsenhofer, R., Frisch, W., Privalov, V., Panova, E., and Spiegel, C. (2010) Thermotectonic evolution of the Ukrainian Donbas Foldbelt revisited: new constraints from zircon and apatite fission track data. *Basin Research*, **22**, 681–698.

Drits, V.A., Zviagina, B.B., McCarty, D.K., and Salyn, A.L. (2010) Factors responsible for crystal-chemical variations in the solid solutions from illite to aluminoceladonite and from glauconite to celadonite. *American Mineralogist*, **95**, 348–361.

Drygant, D. (1993) Conodont colour as indicator of the geological processes (Volyn-Podolia). *Paleontologiceskij Zbirnyk*, **29**, 35–37 (in Ukrainian).

Drygant, D. (2010) *Devonian Conodonts from South-West Margin of the East European Platform (Volyn'-Podolian, Ukraine)*. Academperiodyka, Kyiv, 156 pp (in Ukrainian).

Drygant, D. (2011) Remarks on the geology of the Carpathian Foredeep basement. *Geology and Geochemistry of Combustible Minerals*, **3–4**, 139–155 (in Ukrainian with

English summary).
Dudek, T. and Środoń, J. (1996) Identification of illite/smectite by X-ray powder diffraction taking into account the lognormal distribution of crystal thickness. *Geologica Carpathica–Series Clays*, **5**, 21–32.
Dumitru, T.A. (1993) A new computer automated microscope stage system for fission-track analysis. *Nuclear Tracks and Radiation Measurements*, **21**, 575–580.
Dunkl, I. (2002) TRACKKEY: A Windows program for calculation and graphical presentation of fission track data. *Computer Geoscience*, **28**, 3–12.
Epstein, A.G., Epstein, J.B., and Harris, L.D. (1977) *Conodont Color Alteration – an Index to Organic Metamorphism.* U.S. Geol. Survey Prof. Paper 995, 27 pp.
Franců, J., Muller, P., Šucha, V., and Zatkalikova, V. (1990) Organic matter and clay minerals as indicators of thermal history in the Transcarpathian Depression (East Slovakian Neogene Basin) and the Vienna Basin. *Geologica Carpathica*, **41**, 535–546.
Galbraith, R.F. (1981) On statistical models for fission track counts. *Mathematical Geology*, **13**, 471–438.
Galbraith, R.F. (1990) The radial plot; graphical assessment of spread in ages. *Nuclear Tracks and Radiation Measurements*, **17**, 207–214.
Galbraith, R.F. and Laslett, G.M. (1993) Statistical models for mixed fission track ages. *Nuclear Tracks and Radiation Measurements*, **21**, 459–470.
Gallagher, K., Brown, R., and Johnson, C. (1998) Fission track analysis and its applications to geological problems. *Annual Review of Earth & Planetary Sciences*, **26**, 519–72.
Garetsky, R.G., Zinovenko, G.V., and Vishnyakov, I.B. (1981) Baltic-Dnestrian System of the Pericratonic Depressions. Pp. 44–61 in: *Geology of the Western Part of the East European Platform* (R.G. Garetsky, editor). Minsk, Nauka i Tekhnika.
Gorokhov, I.M., Yakovleva, O.V., Semikhatov, M.A., Mel'nikov, N.N., Ivanovskaya, T.A., and Kutyavin, E.P. (1997) "Rejuvenated" Al-glauconite in Vendian-Cambrian deposits of Podolian Dniester region, Ukraine: Rb-Sr and K-Ar systematics and ^{57}Fe Moessbauer spectra. *Lithology and Mineral Resources*, **32**, 541–558.
Green, P.F. (1981) 'Track-in track' length measurements in annealed apatites. *Nuclear Tracks*, **5**, 12–18.
Green, P.F., Duddy, I.R., Laslett, G.M., Hegarty, K.A., Gleadow, A.J.W., and Lovering, J.F. (1989) Thermal annealing of fission tracks in apatite 4. Quantitative modelling techniques and extention to geological time-scales. *Chemical Geology (Isotope Geoscience Section)*, **79**, 155–182.
Grocholski, A. and Ryka, W. (1995) Carboniferous magmatism of Poland. Pp. 181–190 in: *The Carboniferous System in Poland* (A. Zdanowski and H. Żakowa, editors). Prace Państwowego Instytutu Geologicznego **148**, Warsaw.
Huff, W.D., Bergström, S.M., and Kolata, D.R. (2000) Silurian K-bentonites of the Dnestr Basin, Podolia, Ukraine. *Journal of the Geological Society London*, **157**, 493–504.
Hunziker, J.C., Frey, M., Clauer, N., Dallmeyer, R.D., Friedrichsen, H., Flehmig, W., Hochstrasser, K., Roggwiler, P., and Schwander, H. (1986) The evolution of illite to muscovite: mineralogical and isotopic data from the Glarus Alps, Switzerland. *Contributions to Mineralogy and Petrology*, **92**, 157–180.
Jackson, M.L. (1975) *Soil Chemical Analysis – Advanced Course.* Published by the author, Madison, Wisconsin, USA.
Jaworowski, K. (2002) Geotectonic significance of Carboniferous deposits NW of the Holy Cross Mts. (central Poland). *Geological Quarterly*, **46**, 267–280.
Jeleńska, M., Bakhmutov, V., and Konstantinienko, L. (2005) Paleomagnetic and rock magnetic data from the Silurian succession of the Dniester basin, Ukraine. *Physics of the Earth and Planetary Interiors*, **149**, 307–320.
Karnkowski, P.H. (2003) Carboniferous time in the evolution of the Lublin Basin as the main hydrocarbon formation stage in the Lublin area – results of the geological modelling (PetroMod). *Przegląd Geologiczny*, **51**, 783–790 (in Polish).
Ketcham, R.A., Donelick, R.A., and Donelick, M.B. (2000) AFTSolve: A program for multi-kinetic modeling of apatite fission-track data. *Geological Material Research*, **2**, 1–32.
Kipli, T., Tsegelnjuk, P.D., and Kollaste, T. (2000) Volcanic interbeds in the Silurian of the southwestern part of the East European Platform. *Proceedings Estonian Academy of Sciences, Geology*, **49**, 163–176.
Kornpihl, K. (2005) Tectono-sedimentary evolution of the NE German Variscan foreland basin. PhD thesis, University of Bonn, Germany, 123 pp.
Kowalska, S. (2008) Border of diagenesis and anchimetamorphism in Upper Proterozoic and Cambrian rocks of E part of Małopolska block established by clay mineral studies. PhD thesis, Institute of Geological Sciences PAN, Kraków, Poland, 238 pp.
Kozłowska, A. (2002) Upper Carboniferous sandstone diagenesis in NW part of the Lublin trough. PhD thesis, Polish Geological Institute, Warsaw (in Polish).
Kozłowska, A. (2011) Clay minerals in the Carboniferous sandstones of the southeastern part of the Lublin basin as paleotemperature indicators of diagenesis. *Biuletyn Państwowego Instytutu Geologicznego*, **444**, 99–112 (in Polish).
Krzywiec, P. (2009) Devonian-Cretaceous repeated subsidence and uplift along the Tornquist-Teisseyre Zone in SE Poland ù insight from seismic data interpretation. *Tectonophysics*, **475**, 142–159.
Kübler, B. (1964) Le argiles, indicateurs de metamorphisme. *Revue de l'Institut Francais du Petrole*, **19**, 1093–1112 (in French).
Lindgreen, H., Drits, V.A., Sakharov, B.A., Salyn, A.L., Wrang, P., and Dainyak, L.G. (2000) Illite-smectite structural changes during metamorphism in black Cambrian Alum shales from the Baltic area. *American Mineralogist*, **85**, 1223–1238.
Majorowicz, J., Marek, S., and Znosko, J. (1984) Paleogeothermal gradients by vitrinite reflectance data and their relation to the present geothermal gradient patterns of the Polish Lowland. *Tectonophysics*, **103**, 141–156.
Majorowicz, J.A., Čermak, V., Šafanda, J., Krzywiec, P., Wróblewska, M., Guterch, A., and Grad, M. (2003) Heat flow models across the Trans-European Suture Zone in the area of the POLONAISE'97 seismic experiment. *Physics and Chemistry of the Earth*, **28**, 375–391.
Małkowski, K., Racki, G., Drygant, D., and Szaniawski, H. (2009) Carbon isotope stratigraphy across the Silurian–Devonian transition in Podolia, Ukraine: evidence for a global biogeochemical perturbation. *Geological Magazine*, **146**, 674–689.
McCarty, D.K., Drits, V.A., and Sakharov, B. (2006) Relationship between composition and lattice parameters of some sedimentary dolomite varieties. *European Journal of Mineralogy*, **18**, 611–627.
Moore, D.M. and Reynolds, R.C. (1997) *X-ray Diffraction and the Identification and Analysis of Clay Minerals.* Oxford University Press, Oxford-New York, 378 pp.
Morton, J.P. and Long, L.E. (1984) Rb-Sr ages of glauconite recrystallization: dating times of regional emergence above sea level. *Journal of Sedimentary Petrology*, **54**, 495–506.
Muszyński A., Biernacka J., Lorenc S., Protas A., Urbanek Z., and Wojewoda, J. (1996) Petrology and a depositional environment of Lower Carboniferous rocks near Dygowo

and Kłanino (the Koszalin-Chojnice zone), *Geologos*, **1**, 93–126.

Mystkowski, K., Środoń, J., and McCarty, D.K. (2002) Application of evolutionary programming to automatic XRD quantitative analysis of clay-bearing rocks. *Abstracts with Programs*, The Clay Minerals Society 39th Annual Meeting, Boulder, Colorado, USA, p. 134.

Naeser, C.W. (1981) The fading of fission tracks in the geologic environment – data from deep drill holes. *Nuclear Tracks*, **5**, 248–250.

Nawrocki, J. and Poprawa, P. (2006) Development of Trans-European Suture Zone in Poland: from Ediacaran rifting to Early Palaeozoic accretion. *Geological Quarterly*, **50**, 59–76.

Nehring-Lefeld, M., Modliński, Z., and Swadowska, E. (1997) Thermal evolution of the Ordovician in the western margin of the East-European Platform: CAI and R_o data. *Geological Quarterly*, **41**, 129–138.

Nikishin, A.M., Ziegler, P.A., Stephenson, R.A., Cloetingh, S.A.P.L., Furne, A.V., Fokin, P.A., Ershov, A.V., Bolotov, S.N., Korotaev, M.V., Alekseev, A.S., Gorbachev, V.I., Shipilov, E.V., Lankreijer, A., Bembinova, E.Yu., and Shlimov, I.V. (1996) Late Precambrian to Triassic history of the East European Craton: dynamics of sedimentary basin evolution. *Tectonophysics*, **268**, 23–63.

Nowak, J. (1938) Dniestr a gipsy tortońskie. *Rocznik Polskiego Towarzystwa Geologicznego*, **14**, 155–194 (in Polish).

Paszkowski, M. and Kusiak, M. (2005) Geotectonic aspects of detritus provenance in some Paleozoic epiplatform basins of Poland and adjacent countries. Pp. 11–12 in: *2005 Report of the Institute of Geological Sciences PAS* (in Polish).

Poprawa, P. (2010) Shale gas potential of the Lower Palaeozoic complex in the Baltic and Lublin-Podlasie basins (Poland). *Przegląd Geologiczny*, **58**, 226–249 (in Polish).

Poprawa, P. and Żywiecki, M. (2005) Heat transfer during development of the Lublin basin (SE Poland): maturity modelling and fluid inclusion analysis. *Mineralogical Society of Poland – Special Papers*, **26**, 241–250.

Poprawa, P., Kossakowski, P., and Wróbel, M. (2010) Burial and thermal history of the Polish part of the Baltic region. *Geological Quarterly*, **54**, 131–142.

Pożaryski, W. and Dembowski, Z., editors (1983) *Geological Map of Poland and Adjoining Countries 1:1000000*. Geological Institute, Warsaw.

Reznikov, A.I. (1978) Geological position and general features of flyshoid mass of the middle part of the Donbass. *Geologicheskij Zhurnal*, **38**, 64–72 (in Russian).

Sachsenhofer, R.F and Koltun, Y.V. (2012) Black shales in Ukraine – A review. *Marine and Petroleum Geology*, **31**, 125–136.

Seifert, F. (1968) X-ray powder data for Mg-Al-celadonite (leucophyllite) from Barcza, Poland. *Contributions to Mineralogy and Petrology*, **19**, 93–96.

Shulga, V.F., Zdanowski, A., and Zajceva, L.B. (2007) *Correlation of Carboniferous Coal-bearing Formations of the L'viv-Volyn and Lublin Basins*. National Academy of Sciences of Ukraine and Polish State Geological Institute, Kiev, 427 pp.

Skompski, S., Łuczyński, P., Drygant, D., and Kozłowski, W. (2008) High-energy sedimentary events in lagoonal successions of Upper Silurian of Podolia, Ukraine. *Facies*, **54**, 277–296.

Sliaupa, S., Fokin, P., Lazauskiene, J., and Stephenson, R.A. (2006) The Vendian–Early Palaeozoic sedimentary basins of the East European Craton. Pp. 449–462 in: *European Lithosphere Dynamics* (D.G. Gee and R.A. Stephenson, editors). Memoir **32**, Geological Society, London.

Środoń, J. (1976) Mixed-layer smectite/illites in the bentonites and tonsteins of the Upper Silesian Coal Basin. *Prace Mineralogiczne*, **49**, 84 pp.

Środoń, J. (1984) X-ray powder diffraction identification of illitic materials. *Clays and Clay Minerals*, **32**, 337–349.

Środoń, J. (2007) Illitization of smectite and history of sedimentary basins. *Proceedings of the 11th EUROCLAY Conference*, Aveiro, Portugal, pp. 74–82.

Środoń, J. and Clauer, N. (2001) Diagenetic history of Lower Paleozoic sediments in Pomerania (northern Poland) traced across the Teisseyre-Tornquist tectonic zone using mixed-layer illite-smectite. *Clay Minerals*, **36**, 15–27.

Środoń, J. and Paszkowski, M. (2011) Role of clays in diagenetic history of boron and nitrogen in the Carboniferous of Donbas (Ukraine). *Clay Minerals*, **46**, 561–582.

Środoń, J., Drits, V.A., McCarty, D.K., Hsieh, J.C.C., and Eberl, D.D. (2001) Quantitative XRD analysis of clay-rich rocks from random preparations. *Clays and Clay Minerals*, **49**, 514–528.

Środoń, J., Clauer, N., and Eberl, D.D. (2002) Interpretation of K-Ar dates of illitic clays from sedimentary rocks aided by modeling. *American Mineralogist*, **87**, 1528–1535.

Środoń, J., Kotarba, M., Biroň, A., Šucha, P., Clauer, N., and Wójtowicz, A. (2006a) Diagenetic history of the Podhale-Orava basin and the underlying Tatra sedimentary structural units (Western Carpathians): evidence from XRD and K-Ar of illite-smectite. *Clay Minerals*, **41**, 747–770.

Środoń, J., Clauer, N., Banaś, M., and Wójtowicz, A. (2006b) K-Ar evidence for a Mesozoic thermal event superimposed on burial diagenesis of the Upper Silesia Coal Basin. *Clay Minerals*, **41**, 671–692.

Środoń, J., Clauer, N., Huff, W., Dudek, T., and Banaś, M. (2009a) K-Ar dating of Ordovician bentonites from the Baltic Basin and the Baltic Shield: implications for the role of temperature and time in the illitization of smectite. *Clay Minerals*, **44**, 361–387.

Środoń, J., Zeelmaekers, E., and Derkowski, A. (2009b) The charge of component layers of illite-smectite in bentonites and the nature of end-member illite. *Clays and Clay Minerals*, **57**, 650–672.

Šucha, V., Kraus, I., Gerthofferova, H., Petes, J., and Serekova, M. (1993) Smectite to illite conversion in bentonites and shales of the East Slovak Basin. *Clay Minerals*, **28**, 243–253.

Suggate, R.P. (1998) Relations between depth of burial, vitrinite reflectance and geothermal gradient. *Journal of Petroleum Geology*, **21**, 5–32.

Świdrowska, J., Hakenberg, M., Poluhtoviè, B., Seghedi, A., and Višnâkov, I. (2008) Evolution of the Mesozoic basins on the southwestern edge of the East European Craton (Poland, Ukraine, Moldova, Romania). *Studia Geologica Polonica*, **130**, 3–130.

Tsegelnjuk, P.D. (1980a) *Rukshin and Tsygan series (Lower–Upper Silurian) of Podolia and Volynia*. Preprint 80-2, Inst. Geol. Nauk, Kiev (in Russian).

Tsegelnjuk, P.D. (1980b) *Yaruga and Malinovtsy series (Upper Silurian–Lower Devonian) of Podolia and Volynia*. Preprint 80-11, Inst. Geol. Nauk, Kiev (in Russian).

Ulmishek, G. (1990) Geologic evolution and petroleum resources of the Baltic Basin. *American Association of Petroleum Geologists Memoir*, **51**, 603–632.

Vishnjakov, I.B., Glushko, V.V., and Pomjanovskaja, G.M. (1981) The South-Western Border of the East-European Platform in the Ukraine and Moldavia. Baltic-Dnestrian System of the Pericratonic Depressions. Pp. 22–35 in: *Geology of the Western Part of the East-European Platform* (R.G. Garetsky, editor). Nauka i Tekhnika, Minsk.

Warr, L.N. and Hecht, C.A. (1993) A clay mineral crystallinity investigation of the Upper Carboniferous Culm Basin of south-west England. *Proceedings of the Ussher Society*, **8**, 94–98.

Whitney, G. and Northop, H.R. (1987) Diagenesis and fluid flow in the San Juan Basin, New Mexico – regional zonation in the mineralogy and stable isotope composition of clay minerals in sandstone. *American Journal of Science*, **287**, 253–282.

Wiewióra, A. and Wilamowski, A. (1996) The relationship between composition and *b* for chlorite. *Geologica Carpathica – Series Clays*, **5**, 79–87.

Znosko, J. (1970) Tectonic position of Poland in Europe. *Biuletyn Instytutu Geologicznego*, **251**, 45–70 (in Polish).

(*Received 17 December 2012; revised 12 March 2013; Ms. 735; AE: S. Petit*)